Computational investigation of inverse Heusler compounds for spintronics applications

Jianhua Ma, Jiangang He, Dipanjan Mazumdar, Kamaram Munira, Sahar Keshavarz, Tim Lovorn, C. Wolverton, Avik W. Ghosh, and William H. Butler

Phys. Rev. B **98**, 094410 — Published 10 September 2018

DOI: 10.1103/PhysRevB.98.094410

Computational Investigation of Inverse-Heusler Compounds for Spintronics Applications

Jianhua Ma,[1,*] Jiangang He,[2] Dipanjan Mazumdar,[3] Kamaram Munira,[4] Sahar Keshavarz,[4,5] Tim Lovorn,[4,5] C. Wolverton,[2] Avik W. Ghosh,[1] and William H. Butler[4,5,†]

[1] *Department of Electrical and Computer Engineering, University of Virginia, Charlottesville, VA-22904, USA*
[2] *Department of Materials Science and Engineering, Northwestern University, Evanston, IL 60208, USA*
[3] *Department of Physics, Southern Illinois University, Carbondale, Illinois 62901, USA*
[4] *Center for Materials for Information Technology, University of Alabama, Tuscaloosa, Alabama 35401, USA*
[5] *Department of Physics and Astronomy, University of Alabama, Tuscaloosa, Alabama 35401, USA*

(Dated: August 15, 2018)

First-principles calculations of the electronic structure, magnetism and structural stability of inverse-Heusler compounds with the chemical formula X_2YZ are presented and discussed with a goal of identifying compounds of interest for spintronics. Compounds for which the number of electrons per atom for Y exceed that for X and for which X and Y are each one of the $3d$ elements, Sc-Zn, and Z is one of the group IIIA-VA elements: Al, Ga, In, Si, Ge, Sn, P, As or Sb were considered. The formation energy per atom of each compound was calculated. By comparing our calculated formation energies to those calculated for phases in the Inorganic Crystal Structure Database (ICSD) of observed phases, we estimate that inverse-Heuslers with formation energies within 0.052 eV/atom of the calculated convex hull are reasonably likely to be synthesizable in equilibrium. The observed trends in the formation energy and relative structural stability as the X, Y and Z elements vary are described. In addition to the Slater-Pauling gap after 12 states per formula unit in one of the spin channels, inverse-Heusler phases often have gaps after 9 states or 14 states. We describe the origin and occurrence of these gaps. We identify 14 inverse-Heusler semiconductors, 51 half-metals and 50 near-half-metals with negative formation energy. In addition, our calculations predict 4 half-metals and 6 near-half-metals to lie close to the respective convex hull of stable phases, and thus may be experimentally realized under suitable synthesis conditions, resulting in potential candidates for future spintronics applications.

PACS numbers: 63.22.-m, 66.70.-f, 44.10+i

I. INTRODUCTION

During the past two decades, the field of magneto-electronics and spintronics has experienced significant development[1–3]. Half-metals have the potential to play an important role in the continuing development of spintronics because they have a gap in the Density of States (DOS) at the Fermi energy for one of the spin-channels, but not for the other, creating an opportunity to achieve 100% spin-polarized currents[4, 5]. A half-Heusler compound inspired the term 'half-metal' when, in 1983, de Groot and collaborators calculated the electronic structure of NiMnSb and recognized its unusual electronic structure[6]. Since then, many Heusler compounds have been analyzed and have been theoretically predicted to be half-metals or near-half-metals [7–12].

Due to the near 100% spin polarization at the Fermi level and the relatively high Curie temperatures shown by some Heusler compounds[13–15], half-metallic Heusler compounds have been exploited for devices [16], such as electrodes for magnetic tunnel junctions (MTJs) [17–22], electrodes for giant magnetoresistive spin valves (GMRs)[23–26] and for injection of spins into semiconductors[27].

Heusler-like compounds, sometimes called "inverse-Heuslers" (IH) which are described below can have electronic structures similar to those of the full-Heusler and half-Heusler compounds, in the sense that they may be half-metallic or semiconducting. In addition, the IH compounds can have an electronic structure that has been described as a "spin-gapless semiconductor(SGS)"[28], *i.e.* a large gap at the Fermi energy for one spin channel and a very small gap at the Fermi energy for the other channel.

In this paper we will discuss our survey of IH compounds. We will concentrate on their bulk properties. For many applications heterostructures with interfaces will be needed. These interfaces will affect the electronic structure and transport properties, but are outside the scope of this survey.

The family of Heusler compounds has three subfamilies, the full-Heuslers, the half-Heuslers and the inverse-Heuslers. All three of these subfamilies are based on decorations of atoms and vacancies on an underlying bcc lattice and are most easily visualized by beginning with a bcc lattice represented by the familiar cubic cell

* jm9yq@virginia.edu
† wbutler@mint.ua.edu

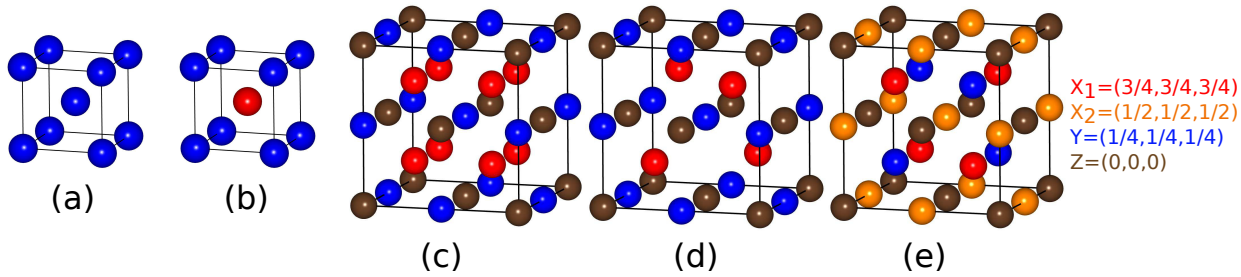

FIG. 1. Schematic representation of full-Heusler $L2_1$ structure and inverse-Heusler XA structure. (a) The *bcc* body-centered cubic structure. (b) The $B2$ cubic structure. (c) The $L2_1$ structure consisting of four interpenetrating fcc sublattices. (d) The half-Heusler $C1_b$ structure consists of three interpenetrating fcc sublattices. (e) The XA structure consists of four interpenetrating fcc sublattices. In the XA structure, X_1 and X_2 are the same transition metal element but they have different environments and magnetic moments.

shown in Figure 1a with all X-type atoms. If the center atom is made different from the atoms at the corners, the structure becomes the $B2$ structure with composition XY (Figure 1b). If, in addition, alternate atoms at the corners in Figure 1b are made different, as shown in the larger cell of Figure 1c, the structure becomes the full-Heusler or $L2_1$ structure with composition X_2YZ. The half-Heusler structure (composition XYZ) can be visualized by removing half of the X atoms from Figure 1c as shown in Figure 1d. The inverse Heusler or XA structure (composition X_2YZ) can be obtained from $L2_1$ by switching one of the X atoms in the $L2_1$ structure with a Y or Z as shown in Figure 1e. In all three families, the X and Y atoms are typically transition metals (at least for the systems that are potential half-metals), while the Z atom is typically an s-p metal.

We have recently completed a survey of the calculated properties of the three subfamilies of Heusler compounds. The results of these calculations are available in a database [29]. We have previously reported on our study of the half-Heusler compounds [30]. In this paper we describe the results of calculations of the properties of IH compounds with particular emphasis on those IH compounds that may be of use for spintronics applications and which may have a reasonable probability of being synthesized.

A universal feature of the electronic structure of Heusler alloys that we consider is the existence of a relatively broad $s-$band followed at higher energy by bands that are primarily derived from $d-$states (Fig. 2). One particular feature of the electronic structure of the IH compounds is especially interesting. The half-Heusler and full-Heusler families often have band gaps after 3 states per atom counting from and including the just mentioned s-band. We call this type of gap a Slater-Pauling gap because Slater and Pauling, but especially Slater, noticed that many bcc based alloys have approximately 3 states per atom in the minority spin channel[31–33]. Furthermore, Slater and Koster showed that for a nearest-neighbor tight-binding model for a B2 alloy (see figure 1) with only d-states, a gap forms in the center of the d-band[31].

The "Slater-Pauling" state for bcc alloys has been ascribed to a minimum in the electronic DOS near the center of the $s-d$ band. This minimum becomes an actual gap after 3 states per atom in one of the spin-channels in some Heusler compounds. In contrast, although many IH compounds show Slater-Pauling gaps at 3 states per atom, some have gaps after a number of states per atom that differs from three.

Thus IH compounds often have gaps after 9, 12, and 14 states per formula unit in the gapped channel. The gap after 12 states corresponds to the Slater-Pauling gap. The gaps after 9 states and 14 states are additional gaps allowed by the reduced symmetry of the inverse-Heusler compared to the full-Heusler. Semiconducting states are possible with half-Heuslers and full-Heuslers, but these typically occur when both spin channels have Slater-Pauling gaps, and both spin-channels are identical implying no magnetic moments on any of the atoms. In contrast, the multiple gaps of the IH compounds allows

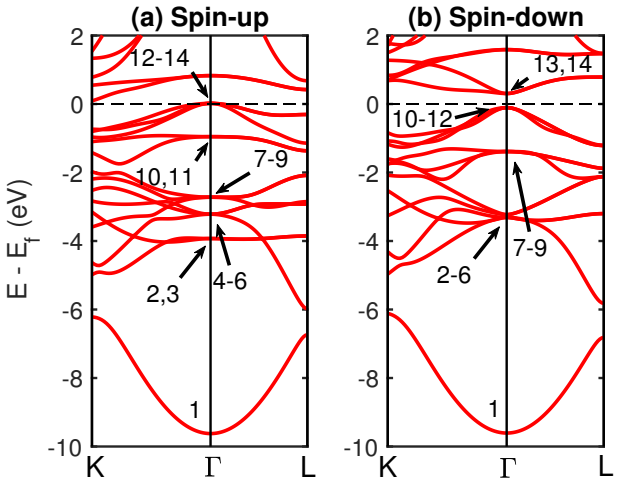

FIG. 2. The band structures of Mn_2CoAl in (a) spin-up and (b) spin-down channels are shown. Bands from 1 to 14 are labeled in (a) and (b). The zero of the energy axis corresponds to the Fermi level.

the possibility of a magnetic semiconductor, *e.g.* when the minority channel has a gap after 12 filled states and the majority has a gap after 14 filled states. The multiple gap possibilities and the possibility of a magnetic semiconductor is illustrated by the partial band structures of Mn_2CoAl shown in Fig. 2. Here it can be seen that the down spin channel has a gap after 12 states per formula unit and the up spin channel has potential gaps after 9 and after 14 states per formula unit. The effect of reduced symmetry on the potential up spin gap after 9 states can be seen in the avoided crossing of bands 9 and 10. For some systems this avoided crossing leaves only a tiny gap. A full explanation of possible band gaps requires an analysis of the band ordering at symmetry points and the symmetry dependent band compatibility relations.

We note that other authors [7, 8, 12, 34] use the term "Slater-Pauling gap" to refer to any gap that can create a half-metal in a Heusler compound. We prefer to reserve the term for gaps after 3 states per atom. We apologize for any confusion our attempt to refine nomenclature may cause.

The reduced-symmetry-derived gaps after 9 and 14 states are often quite narrow so that a state called a spin gapless semiconductor (SGS), a special type of semiconductor in which the Fermi level falls into a relatively large gap in the minority spin-channel (after 12 states) and within a narrow gap for the majority (after 14 states)[34, 35]. This band structure allows both electrons and holes to be excited simultaneously carrying 100% spin polarized current, potentially with high mobility. Recently, the existence of some IH compounds has been confirmed by experiment[36–38]. Additionally, it has been experimentally verified that Mn_2CoAl is an SGS with high Curie temperature[28].

Interestingly, the half-Heusler $C1_b$ phase has the same space group as the inverse-Heusler XA phase and is also prone to gaps after 9 and 14 states per formula unit in a spin-channel. However, in this case 9 states per formula unit coincides with the Slater-Pauling gap after 3 states/atom.

We anticipate that a large and complete database of consistently calculated properties of IH compounds will allow the testing of hypotheses that may explain the occurrence and size of Slater-Pauling band gaps as well as the gaps that occur in some IH compounds after 9 and 14 states per formula unit.

Although a large number of IH compounds have been analyzed by first-principles calculations[12, 34, 39–42], a comprehensive study of the structural, electronic and magnetic properties of the IH family is useful, because it is not clear how many of the IH half-metals and semiconductors that can be imagined are thermodynamically stable in the XA structure. Thus, a systematic study of the structural stability of the IH family can provide guidance for future work.

In Sec. II we describe the details of our computational approach. Sec. II A describes the DFT calculations. In Sec. II B, we discuss how the equilibrium structures for each compound were determined and the possibility of multiple solutions in energy and magnetic configuration for some specific compounds. Our approach to estimating the stability of the IH compounds is described in Sec. II C.

Our results are described in Sections III and IV. Section III describes the formation energies that we calculated for the IH compounds and how these formation energies compare to those of competing phases. Section III A describes a study of the calculated formation energies and stability of those IH phases that have been observed experimentally. The relationship between stability and composition is discussed in Sections III B. Section III C describes our calculated results for the formation energy and stability of the 405 IH compounds that we studied, including an investigation of the relation between gaps at the Fermi energy and stability. Section IV covers the calculated electronic structure of the IH compounds with particular emphasis on those that form semiconductors and half-metals. In Sec. IV A, IH semiconductors, half-metals and near-half-metals with negative formation energy are listed and discussed in terms of their electronic structure and structural stability. Sec. V is a summary of our results and conclusions.

II. COMPUTATIONAL DETAILS AND STRUCTURE DETERMINATION

The IH compound, X_2YZ, crystallizes in the face-centered cubic XA structure with four formula units per cubic unit cell (Fig. 1). Its space group is no. 216, $F\bar{4}3m$, (the same as the half-Heusler). The IH structure can be viewed as four interpenetrating fcc sublattices, occupied by the X, Y and Z elements, respectively. The Z and Y elements are located at the (0, 0, 0) and $\left(\frac{1}{4}, \frac{1}{4}, \frac{1}{4}\right)$ respectively in Wyckoff coordinates, while the X_1 and X_2 elements are at $\left(\frac{3}{4}, \frac{3}{4}, \frac{3}{4}\right)$ and $\left(\frac{1}{2}, \frac{1}{2}, \frac{1}{2}\right)$, respectively, resulting in two different rock-salt structures, $[X_1Y]$ and $[X_2Z]$ as shown in Fig. 1e. We use X_1 and X_2 to distinguish these two X atoms sitting at the two inequivalent sites in the XA structure. Since we also calculated the energy for each compound in the $L2_1$ structure, we also show the $L2_1$ structure in Fig.1c for comparison.

In this study, (a) X is one of 9 elements – Sc, Ti, V, Cr, Mn, Fe, Co, Ni or Cu, (b) Y is one of 9 elements – Ti, V, Cr, Mn, Fe, Co, Ni, Cu, or Zn, and (c) Z is one of 9 elements – Al, Ga, In, Si, Ge, Sn, P, As or Sb. In summary, we calculated the 405 inverse-Heusler compounds for which the valence (or atomic number since X and Y are both assumed to be $3d$) of Y is larger than that of X. For each of these 405 potential IH compounds, we calculated its electronic and magnetic structure, stability against structural distortion, and formation energy. We also compared its formation energy to those of all phases and combinations of phases in the Open Quantum Materials Database (OQMD) [43, 44].

A. Density Functional Theory Calculations

All calculations were performed using density-functional theory (DFT) as implemented in the Vienna Ab-initio Simulation Package (VASP) [45] with a plane wave basis set and projector-augmented wave (PAW) potentials [46]. The set of PAW potentials for all elements and the plane wave energy cutoff of 520 eV for all calculations were both chosen for consistency with the OQMD [43, 44]. The Perdew-Burke-Ernzerhof (PBE) version of the generalized gradient approximation (GGA) to the exchange-correlation functional of DFT was adopted[47]. The integrations over the irreducible Brillouin zone (IBZ) used the automatic mesh generation scheme within VASP with the mesh parameter (the number of k-points per Å^{-1} along each reciprocal lattice vector) set to 50, which usually generated a $15 \times 15 \times 15$ Γ-centered Monkhorst-Pack grid [48], resulting in 288 k-points in the IBZ. The integrations employed the linear tetrahedron method with Blöchl corrections [49]. Finally, All the crystal structures are fully relaxed until the energy change in two successive ionic steps is less than 1×10^{-5} eV.

The total magnetic moment of each compound is calculated by integrating the spin-polarized charge density over the calculation cell. The division of the total magnetic moment among the atoms in the cell is somewhat ambiguous in VASP. The magnetic moment for a particular atom presented in this paper is evaluated within a sphere of 1.45 Å radius centered on the atomic site. It should be noted that the sum of the atomic moments defined this way is not exactly equal to the total cell moment.

B. Determination of the Relaxed Structure

We explain our procedure for obtaining the relaxed structures in some detail in order to make clear that there are many possible structures (in addition to the XA structure) that an X_2YZ compound can assume and that the determination of the ground state can be complicated by the additional degrees of freedom associated with the possible formation of magnetic moments of varying magnitude and relative orientation and by possible distortions of the cell.

We calculated the electronic structure of each compound in the XA phase by minimizing the energy with respect to the lattice constant. For each system and each lattice constant, we found it to be important to initiate the calculation with multiple initial configurations of the magnetic moments. We considered four kinds of initial moment configurations: (1) moments on the 3 transition metal atoms are parallel; (2) moment on the Y site is antiparallel to the moments on the X_1 and X_2; (3) moment on the X_1 site is antiparallel with the moments on the X_2 site and Y; (4) moment on the X_2 site is antiparallel with the moments on the X_1 and Y. After the lattice constant and magnetic configuration that determined the minimum energy for the XA structure was determined we compared this energy to the minimum energy determined in a similar way for the $L2_1$ structure.

Competition between XA and $L2_1$

Comparing the calculated energies of the XA and $L2_1$ phases of the 405 compounds that we considered, we found that 277 have lower energy in the $L2_1$ phase. The remaining 128 have lower energy in the XA phase. This result may be compared to the conclusion in references [12, 40, 50–55] that the XA structure is energetically preferred to the $L2_1$ structure when the atomic number of the Y element is the larger than the atomic number of X. Although this hypothesis is consistent with some experimental observations [37, 38, 40, 56, 57], it does not seem to be generally valid because more than two thirds of the systems in our data set (all of which satisfy $N_Y > N_X$) have lower calculated energy as $L2_1$.

Test for tetragonal distortions via ionic relaxation

After determination of the cubic lattice constant and magnetic configuration in our initial survey, all of the 405 compounds in our survey, both $L2_1$ and XA were tested for stability against tetragonal distortions using an 8 atom tetragonal cell and full ionic relaxation. For both XA and $L2_1$ we considered the structure to be cubic if $|c/a - 1| < 0.01$. All relaxations started from the XA structure or $L2_1$ structure adapted to an 8 atom tetragonal cell.

Of the 277 compounds that preferred the $L2_1$ structure, 136 remained in the $L2_1$ structure while 141 relaxed to a tetragonal '$L2_1$' structure. We notice that few systems with X=Sc, Ti, or V are calculated to be stable as XA. None of the 81 considered compounds with X=Sc were found to be XA. 10 relaxed into the tetragonal '$L2_1$' phase, 63 preferred the $L2_1$ phase and the remaining 8 became tetragonal 'XA' phase. Among the 72 compounds with X=Ti, only 4 compounds preferred XA phase, while 37 relaxed into the tetragonal '$L2_1$' phase, 29 preferred the $L2_1$ phase and 2 distorted to be tetragonal 'XA' phase. Among the 63 compounds with X=V, 43 compounds distorted into tetragonal '$L2_1$' phase, 2 preferred the $L2_1$ phase and 2 distorted to be tetragonal 'XA' phase.

When the 128 compounds that were more stable as XA than $L2_1$ were tested for susceptibility to tetragonal distortion, 95 were found to remain in the XA structure while 33 relaxed to a tetragonal 'XA' phase. In contrast to the half-Heuslers which are prone to trigonal distortions[30], we find that the full-Heuslers and IH compounds tend to retain tetragonal or cubic symmetry during this type of relaxation. The susceptibility of the half-Heuslers to trigonal distortions is likely related to the vacant site in the cell.

If we ignore the competition between XA and $L2_1$ phases, of the 405 potential XA compounds that we considered, 141 were unstable with respect to a tetragonal distortion and the remaining 264 compounds have lower

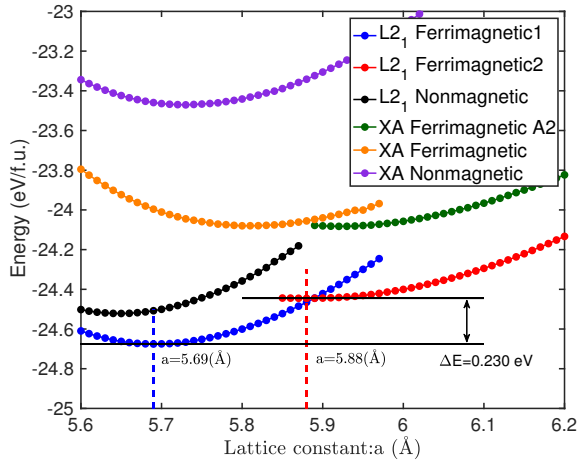

FIG. 3. Calculated total energies of Mn_2ZnP with full-Heusler $L2_1$ structure and inverse-Heusler XA structure as a function of the lattice constant a in ferrimagnetic, ferromagnetic and nonmagnetic states.

energy in XA phase.

Competition between magnetic configurations

For some compounds, we found multiple solutions to the DFT equations at the same or similar lattice constants with different magnetic configurations. These can be categorized into 6 groups: in the $L2_1$ structure; (1) the moments of the X atoms (which are identical by assumption for $L2_1$) are parallel to those for Y ($L2_1$ ferromagnetic), or (2) the moments of X are anti-parallel to those for Y($L2_1$ ferrimagnetic); in the XA structure, (3) the moments for Y are parallel with those for X_1 but anti-parallel with those for X_2 (XA ferrimagnetic A1), or (4) the moments for Y are parallel with those for X_2 but anti-parallel with those for X_1 (XA ferrimagnetic A2), or (5) the moments for X_1 and X_2 are parallel with each other but anti-parallel with those for Y (XA ferrimagnetic), or (6) the moments for X_1, X_2 and Y are parallel (XA ferromagnetic). Magnetic transitions, in both magnitude and orientation as a function of lattice constant are clearly possible and often observed in our calculations. We did not consider the possibility of non-collinear moments[58], and because the calculations did not include spin-orbit coupling, we did not obtain information about the orientation of the moments relative to the crystal axes.

Example Mn_2ZnP

Mn_2ZnP provides an example of competition between different magnetic states for both the $L2_1$ and XA structures as shown in Fig. 3. In this case, the $L2_1$ phases have lower energy. In addition to a nonmagnetic phase with a lattice constant of 5.645Å, two energy minima were found for magnetic phases. These occur at $a = 5.69$ Å and $a = 5.88$ Å. For the solution at $a = 5.69$ Å the total moment per cell is 2.53 μ_B while the moments within a sphere of radius 1.45 Å surrounding each atom are 1.32 for Mn, -0.01 for Zn and -0.10 for P. For the solution at $a = 5.88$ Å the compound has a total magnetic moment of 5.37 μ_B per unit cell, and the moments within the 1.45 Å spheres in this case are 2.75, -0.03, and -0.13 μ_B for Mn, Zn and P, respectively. The solution at $a = 5.88$ Å has higher energy than the solution at 5.69 Å by $\Delta E = 0.230$ eV per formula unit.

There are also multiple XA magnetic phases. The two shown are both ferrimagnetic in the sense that the two Mn moments have opposite signs. The phase with larger lattice constant actually has smaller net moment because of the closer approximate cancellation of the Mn moments.

To be clear, the energy comparisons of the preceding paragraph only consider the XA and $L2_1$ phases and their possible tetragonal distortions. Phase stability is discussed more generally in Section II C.

Competition between ordered and disordered phases

For a few systems, we considered the energy difference between ordered and disordered phases. As will be discussed in detail in Sec.III A, some Mn_2CoZ and Mn_2RuZ XA compounds, (especially when Z is a larger atom, *e.g.* In, Sn, or Sb,) seem to have disorder in the occupation of the Mn_1 and Y sublattice sites. To approximate this disorder in the XA Mn_2CoZ (Z=In, Sn, and Sb) and Mn_2RuSn, special quasi-random structures (SQS) as described by Zunger *et al.* [59] were generated. The SQS are designed to best represent the targeted disordered alloy by a periodic system of a given size.

Our SQS comprised 32 atom cells for the case of completely random (50%/50%) occupation of the X_1 and Y sites, and 64 atom cells for the case in which the X_1 (Y) site occupation was 75%/25% (25%/75%). The SQS was generated using the Monte Carlo algorithm of Van de Walle *et al.* [60] as implemented in the Alloy Theoretic Automated Toolkit (ATAT) [61]. The cluster correlations used to define the SQS were specified using a distance-based cutoff of all 2-, 3-, and 4-body clusters with a maximum distance of 5-6 Å. We did not consider the case with smaller X/Y ratios because much larger unit cells would have been required. More detailed results will be discussed in Sec.III A.

C. Calculation of Energetic Quantities

1. *Formation energy*

We further investigated the structural stability of the 405 potential IH compounds by calculating their formation energies. The formation energy of an IH compound X_2YZ is defined as

$$\Delta E_f\left(X_2YZ\right) = E\left(X_2YZ\right) - \frac{1}{4}\left(2\mu_X + \mu_Y + \mu_Z\right) \quad (1)$$

where $E\left(X_2YZ\right)$ is the total energy per atom of the IH compound, and μ_i is the reference chemical potential of

element i, chosen to be consistent with those used in the OQMD database. Typically the reference energy is the total energy per atom in the elemental phase (see Refs. [43, 44] for details). A negative value of ΔE_f indicates that at zero temperature, the compound is more stable than its constituent elements. It is a *necessary but not sufficient* condition for ground state thermodynamic stability. It does not, for example, guarantee the stability of an inverse-Heusler (IH) phase over another competing phase or mixture of phases. For that, we must determine the convex hull.

2. Convex Hull Distance

A compound can be thermodynamically stable only if it lies *on* the convex hull of formation energies of all phases in the respective chemical space. Every phase on the convex hull has a formation energy lower than any other phase or linear combination of phases in the chemical space at that composition. Thus, any phase on the convex hull is, by definition, thermodynamically stable at 0K. Conversely, any phase that does not lie on the convex hull is thermodynamically unstable; *i.e.* there is another phase or combination of phases on the convex hull that is lower in energy.

The distance from the convex hull $\Delta E_{\rm HD}$ for a phase with formation energy ΔE_f can be calculated as

$$\Delta E_{\rm HD} = \Delta E_f - E_{hull} \quad (2)$$

where E_{hull} is the energy of the convex hull at the composition of the phase. The energy of the convex hull at any composition is given by a linear combination of energies of stable phases. Thus the determination of E_{hull} from a database of formation energies is a linear composition-constrained energy minimization problem[62, 63], and is available as a look-up feature called "grand canonical linear programming"(GCLP) on the OQMD website (http://oqmd.org/analysis/gclp). Obviously, if the hull distance $\Delta E_{\rm HD}$ for a phase on the convex hull is 0, there is no other phase or linear combination of phases lower in energy than the phase at that composition. The distance of the formation energy of a phase from the convex hull is an indicator of its thermodynamic stability and the likelihood of it being fabricated because the greater the distance from the convex hull, the higher is the thermodynamic driving force for transformation into another phase or decomposition into a combination of phases.

We note that the distance of a phase from the calculated convex hull depends on the completeness of the set of phases considered in the construction of the convex hull. Ideally, to calculate the convex hull of a system, X-Y-Z, one would calculate the energies of all possible compounds that can be formed from elements X, Y, and Z. Unfortunately, such a comprehensive study is not currently feasible.

A practical approach is to construct the convex hull using all the currently reported compounds in the X-Y-Z phase space. Here, we have limited our set of considered phases to those in the OQMD, which includes many ternary phases that have been reported in the ICSD[64, 65], and $\sim$ 500,000 hypothetical compounds based on common crystal structures. Thus the calculated formation energy of each X_2YZ IH compound is compared against the calculated formation energies of all phases and all linear combinations of phases with total composition X_2YZ in the OQMD.

A phase that we calculate to be above the convex hull may still be realized experimentally for three reasons: (a) There may be errors in the calculation of the energies of the IH compound or in the reference compounds. These errors may be intrinsic to PBE-DFT or due to insufficient precision in the calculation or inability to distinguish the ground state. We have applied considerable effort to reduce or eliminate the latter two possibilities so far as possible. (b) The compounds are usually synthesized at temperatures well above 0K. Because entropic effects will differ for different phases, the phase with lowest free energy at the synthesis temperature may be different from the phase with lowest energy at 0K and this high temperature phase may persist to low temperature due to slow kinetics at laboratory time scales. (c) Non-equilibrium processing techniques can sometimes be used to fabricate non-equilibrium metastable phases.

Conversely, an IH phase that we calculate to be on the calculated convex hull may nevertheless be difficult or impossible to fabricate because of reasons (a) or (b) or because the database used to generate the convex hull does not contain all phases so that the true convex hull lies below the calculated one.

Finally, we remark that our stability investigations are most directly pertinent to bulk phases. The growth of alloy films is a sophisticated art. Phases that are stable in bulk can be difficult to grow as films. Conversely, clever use of substrates, surface energies and kinetics can stabilize film structures different from the equilibrium bulk phase. Even for films, however, the hull distances provided here may provide useful guidance concerning the likelihood that a phase or structure may be stabilized.

III. FORMATION ENERGY AND STABILITY

A. Formation Energy and Convex Hull Distance

In this section, we systematically investigate the formation energy and thermodynamic stability of the 405 IH compounds considered in this paper. The formation energies at 0 K were evaluated by using Eq. (1) and the convex hull distances were calculated using Eq. (2). We first explored the relationship between formation energy and convex hull distance for the known synthesized IH compounds, including those collected in the Inorganic Crystal Structure Database (ICSD).

We compiled a list of the reported IH compounds by extracting IH compounds from the ICSD and literature including all elements as potential X, Y or Z atoms. From this list we removed the compounds with partially occupied sites. Some of the ICSD entries were from DFT calculations. These were included except for those with a higher DFT energy than the corresponding full Heusler which were obviously included in the ICSD by mistake. Finally, we tabulated the formation energy and convex hull distance as calculated in the OQMD.

A total of 48 distinct IH compounds are reported in ICSD. Of these, 36 have been synthesized experimentally. References to six additional synthesized IH compounds, not included in ICSD, (Fe_2CoGa, Fe_2CoSi, Fe_2CoGe, Fe_2NiGa, Mn_2NiGa, and Fe_2RuSi) were found in recent literature [66, 67]. These can be used for cross validation of our method. Although Mn_2NiSn was synthesized by Luo *et al.* [68], a more recent study shows that it has atomic disorder on the transition metal sites [67] and our DFT calculation show it is 103 meV/atom above the convex hull.

These data from ICSD and the recent literature are displayed in Fig. 4, from which it can be seen that most of the synthesized IH compounds are within 52 meV/atom of the convex hull. The green diamonds represent the IH compounds that have not been synthesized but have been sourced into the ICSD by DFT predictions.

Overall, we find most of the experimentally reported IH compounds (38 of 42) have a convex hull distance less than 52 meV/atom. Thus, the convex hull distance of the DFT-calculated formation energy at 0K appears to be a good indicator of the likelihood of synthesis of an IH compound and 52 meV/atom is a reasonable empirical threshold separating the compounds likely to be synthesized by equilibrium processing from those unlikely to be so synthesized.

The empirical 52 meV threshold assumed here may be contrasted with the 100 meV threshold that seemed appropriate for the half-Heusler compounds [30]. We speculate that the more open structure of the half-Heusler phase is associated with a high density of states for low frequency phonons which reduces the free energy of the half-Heusler phase relative to competing phases at temperatures used for synthesis.

Before proceeding it is important to note that several Mn_2YZ compounds (Mn_2CoSn, Mn_2CoSb, Mn_2CoIn, and Mn_2RuSn) appear to significantly violate our empirical hull distance threshold. They also have vanishing or positive formation energy! A discussion of our rationale for *not* extending our hull distance threshold to include these systems follows:

(a) Mn_2CoSn: Our calculations predict that XA phase Mn_2CoSn lies well above the convex hull. A mixture of phases, CoSn-Mn is predicted to be lower in energy by $\Delta E_{\rm HD} = 0.107$ eV/atom. However, there are reasons to believe that the experimentally reported phase may not be pure XA.

The ICSD entry for Mn_2CoSn is based on the work

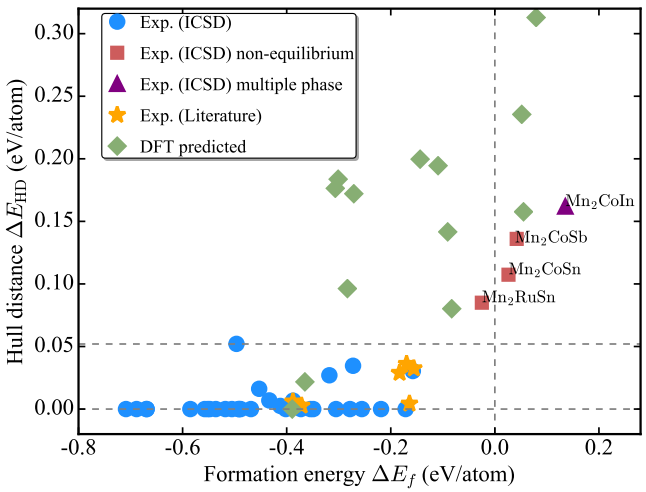

FIG. 4. DFT-calculated formation energy vs. convex hull distance of inverse Heuslers reported in ICSD and in recent experimental studies. A hull distance $\Delta E_{\rm HD}$=0 (on the convex hull) indicates the compound is thermodynamically stable at 0K. Blue circles and red squares represent experimentally synthesized IH through equilibrium and non-equilibrium process, respectively. Purple triangle is synthesized IH coexisting with other phase. Yellow stars represent synthesized compounds reported in literature but not in ICSD. Green diamonds represent IH compounds predicted using DFT.

of Liu *et al.* who described synthesis via melt-spinning as well as calculations that employed the FLAPW technique [40]. They found that the non-equilibrium melt-spinning technique generated a material with a "clean" XRD pattern consistent with the XA phase. The measured magnetic moment of 2.98 μ_B per formula unit was consistent with their calculated value of 2.99 and with their calculated DOS, which indicates that this material may be a Slater-Pauling near-half-metal.

Subsequently, Winterlik *et al.* synthesized this compound by the quenching from 1073K of annealed arc-melted samples[38]. They obtained similar XRD results to Liu *et al.*, but with a small admixture of a tetragonal $MnSn_2$ phase. They also concluded that the experimental moment was near the Slater-Pauling half-metal value of 3 μ_B per formula unit. However, their calculations for XA-phase Mn_2CoSn which also employed FLAPW found, in addition to the near-half-metallic phase found by Liu *et al.*, a different magnetic structure with lower energy.

Our calculations using VASP confirm the Winterlik *et al.* results. The PBE-DFT-predicted phase for XA Mn_2CoSn has a magnetic moment around 1.53 μ_B rather far from the value of 3 μ_B necessary to place the Fermi energy into the Slater-Pauling gap after 12 states per atom in the minority channel. There is an interesting competition between two very similar ferrimagnetic states that plays out in many of the 26 and 27 electron Mn_2CoZ systems. The Mn_2 and Co moments are aligned and are partially compensated by the Mn_1 moment. For

smaller lattice constants, the compensation yields the correct moment for a half-metal or near-half-metal (i.e., for Mn_2Co(Al,Ga,Si,Ge)), but as the lattice constant increases, (*i.e.,* for Mn_2Co(In,Sn)), the Mn_1 moment becomes too large in magnitude and the partial compensation fails to yield a half-metal.

Winterlik *et al.* conclude from XRD, NMR and Mössbauer studies that their quenched samples of Mn_2CoSn are actually disordered on the MnCo layers. They modeled this disorder using the KKR-CPA approach and obtained values of the moments in reasonable agreement with magnetometry and XMCD. They argued that their model with Mn and Co randomly occupying the sites on alternate (001) layers separated by ordered Mn-Sn layers agreed with XRD as well as the XA model because Mn and Co scatter X-rays similarly. This disordered $L2_1B$ structure has both Mn and Co at the $\left(\frac{1}{4}, \frac{1}{4}, \frac{1}{4}\right)$ and the $\left(\frac{3}{4}, \frac{3}{4}, \frac{3}{4}\right)$ site, whereas the XA structure has only Co at $\left(\frac{1}{4}, \frac{1}{4}, \frac{1}{4}\right)$ and only Mn at $\left(\frac{3}{4}, \frac{3}{4}, \frac{3}{4}\right)$ site.

We investigated the Winterlik *et al.* hypothesis by comparing the energy of a few cubic 16 atom supercells with differing equiatomic occupations of the MnCo layers to the energy of the XA occupation. The energies of these different site occupations were all lower than the XA energy, and most of them were half-metallic or near-half-metallic. The decrease in energy for the non-XA site occupations ranged from 8 meV/atom to 33 meV/atom. These should be considered lower bound estimates of the decrease since we did not optimize the geometries of the model "disordered" structures. We also performed calculations for an SQS designed to mimic a system with disorder on the MnCo layers. Our calculation indicates that the SQS with 25% Mn/Co mixing is 31 meV/atom lower in energy than the XA phase. The net magnetic moment of this SQS is about 1.28 μ_B per f.u., which is lower than that of XA phase (1.53 μ_B) due to the atom disordering.

We propose the following hypothesis and rationale for omitting Mn_2CoSn from the estimate for the hull energy distance threshold: During synthesis at high temperature, Mn_2CoSn is thermodynamically stable in a phase with substantial configurational disorder on the MnCo planes. The configurational disorder on these sites may also decrease the free energy of the compound. A simple mean-field estimate of the configurational entropy (S) of disorder gives a $-TS$ contribution of -32 meV/atom at 1073K. If we add this entropic contribution to the approximately 30 meV/atom difference in total energy between the ordered and disordered systems, we can estimate a decrease in the relative free energy of formation by approximately 60 meV/atom due to disorder. This would yield a negative free energy and a hull distance less than our empirical 52 meV threshold.

(b) Mn_2CoSb: Mn_2CoSb is predicted to lie above the convex hull with a mixture of phases CoMnSb-Mn lower in energy by $\Delta E_{\mathrm{HD}} = 0.133$ eV/atom. This phase also entered the ICSD database from the paper of Liu *et al.* who generated their sample by melt-spinning and also provided FLAPW calculations that predicted XA Mn_2CoSb to be a half-metal with a Slater-Pauling moment of 4 μ_B per formula unit, consistent with their measured value.

Unlike some Mn_2CoZ compounds with smaller Z atoms, synthesis of single XA phase Mn_2CoSb is difficult via arc-melting and a high temperature annealing step. Prior X-ray diffraction investigations [40] revealed a multi-phase Mn_2CoSb in arc-melt samples. Our synthesis supports this finding [69]. On the other hand, a melt-spinning treatment of arc-melt Mn_2CoSb ingots is reported to produce a pure cubic structure [40, 70].

We consider it likely that Mn_2CoSb is similar to Mn_2CoSn. A study by Xin *et al.* found that "disordered" Mn_2CoSb (apparently modeled by replacing the (001) MnCo layers by layers of pure Mn and pure Co alternating with the MnSb layers) was lower in energy than XA by 21 meV/atom [39]. Our SQS calculations show that the 50% Mn/Co mixture within one rock-salt lattice is 60 meV/atom lower in energy than the XA phases. Again, our assertion is that the free energy reduction due to configurational entropy together with the lower energy of the disordered configurations may be sufficient to stabilize the $L2_1B$ phase as it is rapidly quenched from the melt.

(c) Mn_2CoIn: According to Liu *et al.*[40], Mn_2CoIn appears to be multi-phase in samples prepared by arc-melting. Apart from the cubic phase identified as inverse-Heusler, a second phase described as fcc is also apparent. Liu *et al.* also report FLAPW calculations performed at a much smaller lattice constant (5.8 Å) than the experimentally derived lattice constant (6.14 Å). These calculations yielded a moment of 1.95 μ_B in reasonable agreement with experimental value of 1.90 μ_B. A subsequent calculation by Meinert *et al.* found a lattice constant of 6.04 Å and a moment of 1.95 μ_B[52].

Our calculations for the XA phase yielded a lattice constant of 6.10 Å, much closer to the experimental value and a moment of 1.74 μ_B. We also found a surprising and unusual sensitivity of our results to the number of plane waves. We performed SQS calculations which indicated that the disordered phase is essentially degenerate in energy with the XA phase. The magnetic moment of SQS is about 1.01 μ_B per f.u..

Given the significant amount of second phase in the experimental sample which would affect the composition of the phase identified as XA, together with the possibility of disorder on the MnCo layers we tentatively conclude that it is reasonable to discount the large calculated formation energy and hull distance in setting our threshold for likely fabricability of XA phases . Additional studies of this putative phase are probably advisable.

(d) Mn_2RuSn: Mn_2RuSn is predicted to lie above the convex hull with a mixture of phases MnSnRu+Mn+Sn_7Ru_3 by $\Delta E_{\mathrm{HD}} = 0.085$ eV/atom. The first reports of fabrication by Endo *et al.*[71], were unable to distinguish between the XA and $L2_1B$ phases.

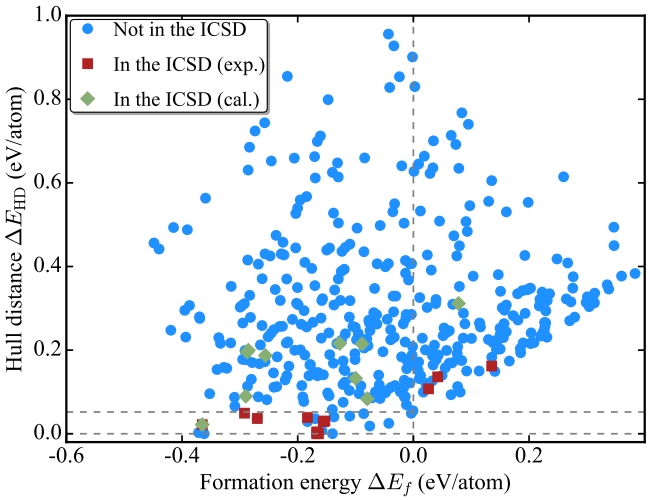

FIG. 5. DFT-calculated formation energy vs convex hull distance of all IH considered in this paper. A hull distance $\Delta E_{\rm HD}$=0 (on the convex hull) indicates the compound is thermodynamically stable at 0K. Red diamonds and green squares represent IH compounds sourced into ICSD by synthesis and DFT computation, respectively. Blue circles represent the IH compounds calculated in this work.

A later study by Kreiner *et al.* seemed to confidently conclude from powder XRD studies that their sample prepared by alloying through inductive heating had the $L2_1B$ structure[67]. Our calculation of the energy of a SQS for Mn_2RuSn with 25% Mn/Ru mixing gave an energy of the model disordered alloy 18 meV lower than XA. The calculated magnetic moment of the SQS is about 0.24 μ_B per f.u.. A study by Yang *et al.* using the KKR -CPA approach estimated 11% anti-site Mn based on a comparison of the calculated moment to the experimental one[72].

We tentatively conclude that the four experimental systems in the ICSD with anomalously large calculated hull distances and formation energies are probably not XA phase and exclude them from consideration in determining the threshold for estimating which XA phases are likely to be fabricated by equilibrium approaches. We also remind that an additional potential inverse-Heusler, Mn_2NiSn, was excluded from our database of experimental XA phases, because of experimental evidence of similar disorder to that observed in the Mn_2CoZ phases.

We recommend additional studies of the competition between XA and $L2_1B$ phases, especially for compounds which have large Z atoms. Such studies may require careful experimental analysis because of the similarities of the the XRD patterns of the two phases. Theoretical studies may also be difficult because of the need to accurately calculate the formation energy of the disordered $L2_1B$ phase.

We extended the comparison of formation energy and convex hull distance to all the 405 IH compounds considered in this work as shown in Figure 5. It can be seen from Fig. 5 that the calculated formation energies span a range from -0.45 to 0.38 eV/atom. This may be compared with a range of -1.1 to 0.7 eV/atom that was observed for half-Heuslers [30]. 248 of the IH have negative formation energy, indicating thermal stability against decomposition into the constituent elements at 0 K. The calculated hull distances vary from 0 to nearly 1 eV/atom. It is clear from the lack of correlation between formation energy and hull distance in Figure 5 that the formation energy is not a reliable indicator of stability.

The IH compounds considered in this work that are included in ICSD are indicated by red squares in Figure 5. These all lie within 0.052 eV/atom of the convex hull except for three compounds mentioned previously (Mn_2CoSn, Mn_2CoIn and Mn_2CoSb) that were synthesized by non-equilibrium processing and are likely $L2_1B$ rather than XA phase. Our calculations predict 13 (out of 405) IH compounds to be within 52 meV/atom of the convex hull. The "success rate", i.e. the number of predicted potentially stable compounds versus total number of systems investigated is lower for IH (13/405) than for half-Heusler (50/378) [30], but this result is affected by the different hull distance thresholds and the different choices of potential compounds.

B. Stability and Composition

We systematically investigated the formation energies of the 405 IH compounds in the XA phase. We found that many of these potential IH phases actually have lower energy in other phases, *e.g.* $L2_1$(136), tetragonal '$L2_1$' phase (141), or tetragonal 'XA(33). Here, however, since we are interested in gaining insight into the systematics of the stability of the XA phase, we compare formation energies as if all 405 compounds remained in the XA phase. To better illustrate the relation between structural stability and composition, we arranged the formation energy data according to X, Y and Z element respectively in Fig. 6-8.

Figure 6 shows the calculated formation energies and hull distances of the 405 calculated X_2YZ compounds arranged by X species, then by Y and finally by Z. From Fig. 6, we can see that Sc, Ti, and V generate more negative formation energy XA compounds as X elements. In terms of the fraction with negative formation energy, we found 75/81 with X=Sc, 60/72 with X=Ti, 25/45 with X=Mn and 20/36 with X=Fe, and 15/18 with X=Ni.

Figure 7 presents the calculated formation energies and hull distances arranged first by Y, then by X and finally by Z. From Fig. 7, it can be seen that when Y is Fe, Co or Ni many XA compounds with negative formation energies result. However, when one considers the fraction of negative formation energy compounds with a given Y in our database, the highest are 9/9 for Y=Ti, 17/18 for Y=V and 24/27 for Y=Cr.

When the compounds are ordered by Z element as presented in Fig. 8, we can see that the smaller atoms within a given group (*i.e.* Z=Al, Si, In) tend to have a larger

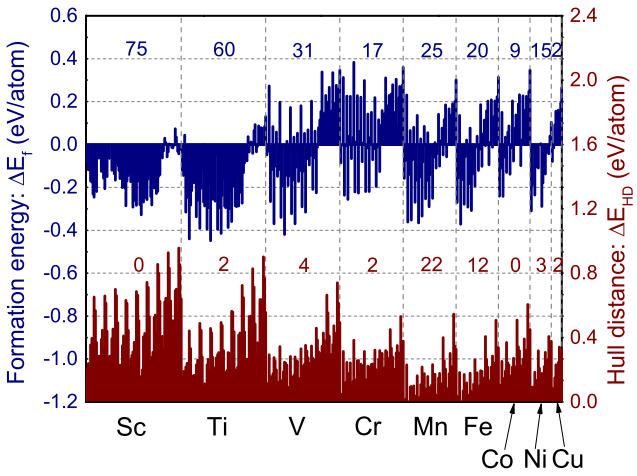

FIG. 6. DFT formation energies and hull distances for potential inverse-Heusler compounds grouped by the element on the X-site. The numbers near the top (in blue) and center (in brown) of each column denote the number of compounds with negative formation energy ΔE_f and hull distance $\Delta E_{\rm HD} \leq 0.1$ eV/atom, respectively, in the corresponding Z-element group. Within a given X-element column, the compounds are ordered first by the element on the Y-site (same order as in Fig. 7) and then by the element on the Z-site (same order as in Fig. 8), i.e., Z varies more rapidly than Y.

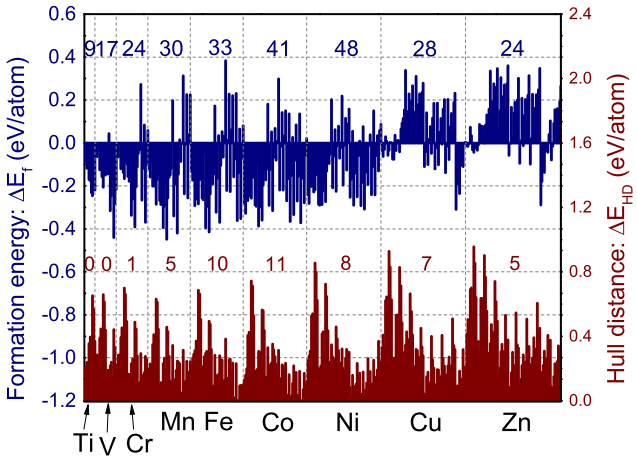

FIG. 7. DFT formation energies and hull distances for potential inverse-Heusler compounds grouped by the element on the Y-site. The numbers near the top (in blue) and center (in brown) of each column denote the number of compounds with negative formation energy ΔE_f and hull distance $\Delta E_{\rm HD} \leq 0.1$ eV/atom, respectively, in the corresponding Y-element group. Within a given Y-element column, the compounds are ordered first by the element on the X-site (same order as in Fig. 6) and then by the element on the Z-site (same order as in Fig. 8), i.e., Z varies more rapidly than X.

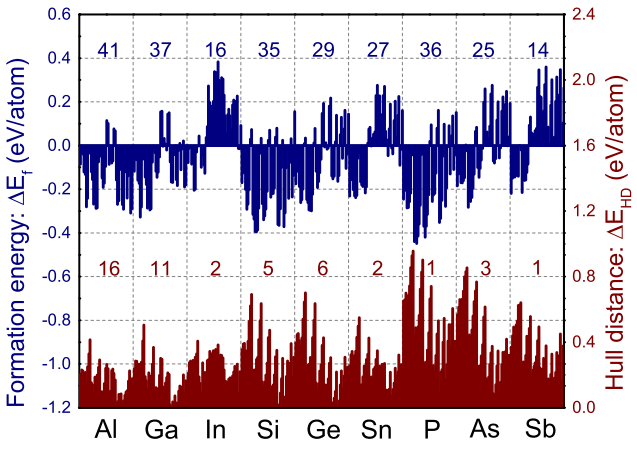

FIG. 8. DFT formation energies and hull distances for potential inverse-Heusler compounds grouped by the element on the Z-site. The numbers near the top (in blue) and center (in brown) of each column denote the number of compounds with negative formation energy ΔE_f and hull distance $\Delta E_{\rm HD} \leq 0.1$ eV/atom, respectively, in the corresponding Z-element group. Within a given Z-element column, the compounds are ordered first by the element on the X-site (same order as in Fig. 6) and then by the element on the Y-site (same order as in Fig. 7), i.e., Y varies more rapidly than X.

fraction of negative energy XA phases. The large number of $\Delta E_f < 0$ compounds with Z=Al is striking in Fig.8, but only 14 compounds have negative formation energy for Z=Sb. Although the number of negative formation energy compounds with Z=Al is greatest, the number among them with formation energies less than -0.2 eV (13) is less than for compounds with Z=Si (25) and Z=P (24).

It is interesting to contrast the trends in formation energy to those observed by considering the OQMD hull distance. Although Sc, and Ti tend to generate negative formation energies as X atoms in XA phase X_2YZ compounds, the picture is opposite for the hull distances. Very few of these compounds have a hull distance near the empirical 0.052 eV/atom range which is indicative of a potentially synthesizable phase. Using a larger hull distance of 0.1 eV as an (arbitrary) stability threshold we find no X=Sc phases that meet the criterion and only 2 of 72 X=Ti phases. Sc and Ti are "active" elements that form numerous low energy phases. Hull distances tend to be lower when the X atom is Mn or Fe with 22 of 45 X=Mn and 12 of 36 X=Fe meeting the criterion of hull distance less than 0.1eV/atom.

While 9/9 Y=Ti and 17/18 Y=V IH compounds have negative formation energy, none of them meet the relaxed hull distance threshold of 0.1eV/atom. However, relatively large fractions of Y=Fe (10/45), Y=Co (11/45) and Y=Ni (8/63) meet the criterion. Thus, there is better correlation between low formation energy and low hull distance when the XA compounds are grouped by Y element. By both measures, Y=Ni, Co or Fe tend to gen-

erate more stable compounds.

The trends in stability with Z atom are also somewhat similar when viewed from the perspectives of hull distance and formation energy. Al, Ga, Si and Ge as Z atom are associated with compounds having relatively low hull distances and negative formation energies. One big difference, however, is Z=P which tends to generate numerous XA compounds with low formation energy, but none with very low hull distances.

C. Stability and Gaps near the Fermi Energy

We calculated the electronic structure of each compound and obtained its spin polarization at the Fermi level, E_F. The spin polarization P at E_F is defined as:

$$P(E_F) = \frac{N_\uparrow(E_F) - N_\downarrow(E_F)}{N_\uparrow(E_F) + N_\downarrow(E_F)} \quad (3)$$

where $N_\uparrow$ and $N_\downarrow$ are the densities of states for majority (spin-up) and minority (spin-down) electrons, respectively. We define the compounds with 100% spin polarization ($P(E_F) = 1$) to be half-metals in this paper.

In a study of the half-Heusler compounds gaps at the Fermi energy in one or both spin channels appeared to be associated with low formation energies and low hull distances[30]. Figure 9 shows how the number of IH compounds with positive and negative formation energy varies with spin-polarization. It can be seen that for semiconductors and half-metals the ratio of the number of negative formation energy compounds to positive formation energy compounds is particularly high.

Figure 10 shows the number of IH compounds with positive and negative hull distances less than and greater than 0.1 eV/atom versus spin polarization. In contrast to the case of the half-Heuslers, the plot of hull distance versus spin-polarization does not present an obvious case for a correlation between gaps near the Fermi energy and stability. As will be discussed in Section IV A, this is due to the large number of X=Sc and X=Ti compounds in our database that are semi-conductors or half-metals and although they tend to have negative formation energies, they tend to be less stable than competing compounds. On the other hand, as will be discussed in Sec. III, only 20 of the IH compounds in our database systems met our 0.052 eV/atom hull distance stability criterion. Half of these are half-metals or near-half-metals. We consider this to be strong support for the notion that gaps in or near the Fermi energy in one or both spin channels contribute to stability.

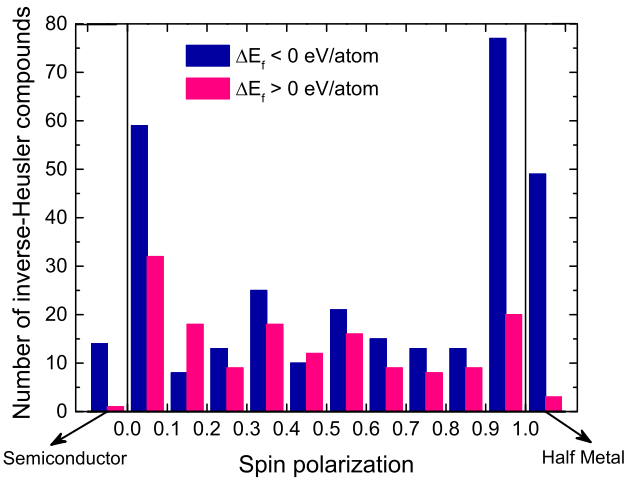

FIG. 9. The distribution of the 405 potential inverse-Heusler compounds with negative ($\Delta E_f < 0$ eV/atom) and positive ($\Delta E_f > 0$ eV/atom) formation energies as a function of spin polarization $P(E_F)$ (given by Eq. 3). In the central region, we show the number of inverse-Heusler compounds grouped by 10 percentage points of spin polarization. In an additional region to the left, we show the 15 semiconductors, including 14 compounds with a negative formation energy and 1 with a positive formation energy. In the additional region on the right, we show 52 half-metals, including 51 with negative formation energy and 1 with positive formation energy.

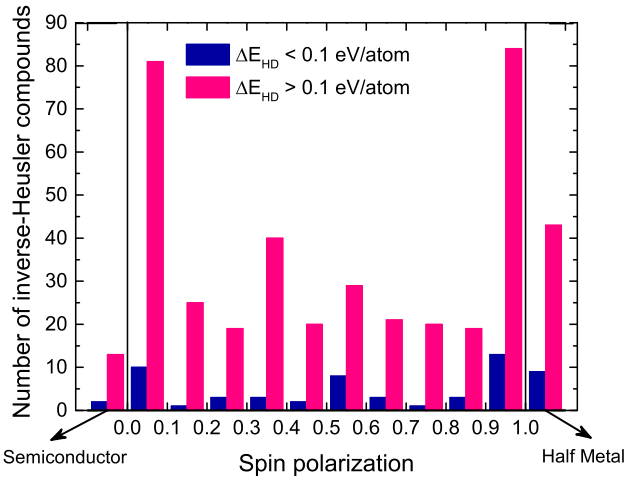

FIG. 10. The distribution of the 405 potential inverse-Heusler compounds that lie near ($\Delta E_{\rm HD} < 0.1$ eV/atom) or far ($\Delta E_{\rm HD} > 0.1$ eV/atom) from the convex hull, as a function of spin polarization $P(E_F)$ (given by Eq. 3). In the central region, the number of inverse-Heusler compounds grouped by 10 percentage points of spin polarization is shown. In the additional region on the left are shown 15 semiconductors (of which 2 compounds have $E_{\rm HD} < 0.1$ eV/atom). On the right are shown the 52 half-metals (of which 9 compounds have $E_{\rm HD} < 0.1$ eV/atom).

IV. ELECTRONIC STRUCTURE

In this section the electronic structures of the IH compounds are discussed with a particular emphasis on gaps in the density of states, particularly those after 9, 12 and 14 states per formula unit.

A. IH Semiconductors and half-metallic ferromagnets

In total we found 14 semiconductors, 51 half-metals, and 50 near-half-metals with negative formation energy among the 405 potential IH compounds. We will discuss these materials in this section.

1. *Semiconductors*

The 14 XA semiconductors with negative formation energy that we found are listed in Table I where the DFT-calculated properties (*i.e.* lattice constant, band gap, gap type, local moments, formation energy, hull distance) are presented. Remarkably, all of these 14 systems are 18 electron *non-Slater-Pauling* semiconductors with gaps after nine electrons per formula unit (2.25 per atom) per spin channel. Recall that *Slater-Pauling* gaps (at least according to the nomenclature we prefer) occur after 3 electrons per atom per spin.

From Table I, it can be seen that all of these semiconductors have either Sc or Ti as X atoms. This is not surprising (given that they all have 18 electrons per formula unit) because the choice of systems that comprise our database (see section II) implies that if the number of valence electrons on an X atom exceeds 4, the total number of electrons per formula unit will exceed 18.

Of the 9 XA compounds with X=Sc in our database, 7 are calculated to be non-magnetic semiconductors. The two that are not semiconductors are Sc_2MnAs and Sc_2MnSb. The former is non-magnetic with a very low DOS pseudogap at the Fermi energy.

The absence of a gap in Sc_2MnAs can be traced to a reordering of the states at Γ. Between Sc_2MnP and Sc_2MnAs, a singly degenerate A_1 state (band 7) switches places with a triply degenerate T_2 state (bands 8,9 and 10), as shown in Fig. 12. This A_1 state (composed of s-contributions from all 4 atoms) decreases in energy relative to the d-states as the lattice expands from Sc_2MnP to Sc_2MnAs to Sc_2MnSb. However, Sc_2MnSb becomes magnetic as the lattice is expanded before this reordering occurs so it is predicted to be a magnetic near-half-metal with a tiny moment (see Table III).

The reason Sc_2MnSb is magnetic while Sc_2MnP and Sc_2MnAs are not is almost certainly due to the larger lattice constant induced by the larger atom (Sb). For lattice constants less than approximately 6.50 Å, Sc_2MnSb is predicted to be a non-magnetic semiconductor similar to Sc_2MnP.

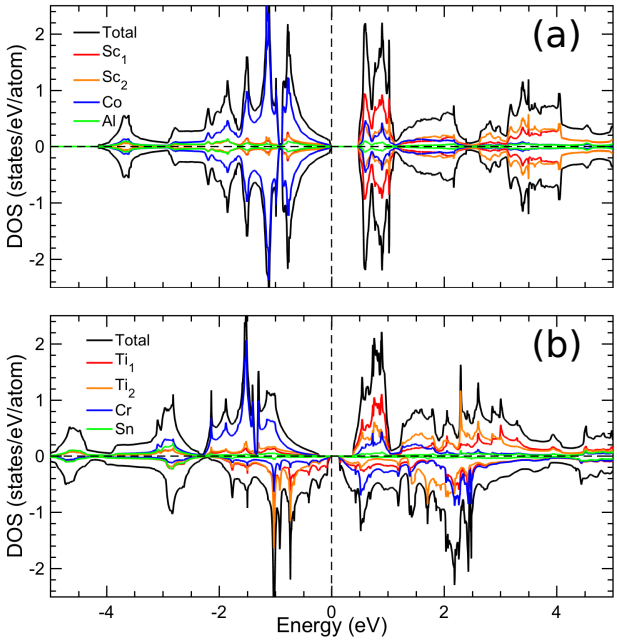

FIG. 11. Density of states curves for the 18-electron semiconductor (a) Sc_2CoAl and (b) Ti_2CrSn. The curve presents the total DOS (black) and the projected-DOS contributed by Sc_1 (Ti_1) (red), Sc_2 (Ti_2) (orange), Co (Cr) (blue) and Al (Sn) (green). Zero energy corresponds to the Fermi level.

The DOS of the non-magnetic Sc-based semiconductors in Table I can be understood by referring to Figure 11a which shows the site decomposed DOS for Sc_2CoAl. Because Sc is an early transition metal compared to Co, its d-states must lie higher. Thus, the ordering of the states is Al-s (in this case forming a narrow band well below the Fermi level and not shown in the figure.) followed by Al-p, followed by Co-d and finally Sc_1-d and Sc_2-d. The gap after 9 electrons per spin channel occurs from the hybridization of the Co-d and Sc-d states, or, more generally, between the Y-d and X-d states.

Thus, bonding in these systems appears to have a considerable ionic component with transfer of electrons to the Al and Co atoms from the Sc atoms.It can be seen from Table I that all of the X=Sc 18-electron semiconductors are predicted to be substantially more stable in the $L2_1$ phase than in the XA phase. In addition, the XA hull distances all exceed our 0.052 eV threshold for potentially being stable in equilibrium.

Of the nine 18 electron compounds in our database with X=Ti, seven are predicted to be semiconductors and are included in Table I. One, Ti_2VP is predicted to be a near-half-metal (see Table III) with a tiny moment. The final compound, Ti_2VAs, is predicted to be a magnetic semiconductor similar to Ti_2VSb, but its formation energy is greater than zero and so is omitted from Table I.

In contrast to the non-magnetic 18 electron semiconductors with X=Sc, the systems with X=Ti develop

TABLE I. For each of the 14 18-electron X_2YZ inverse-Heusler compounds that are non-Slater-Pauling semiconductors with negative formation energy, we list the calculated lattice constant a, band gap in two spin channels $E_g^{\uparrow}$, $E_g^{\downarrow}$ within DFT, local moments for atoms on the X, Y and Z sites:$m(X_1)$, $m(X_2)$, $m(Y)$ and $m(Z)$, the formation energy of the compound in the XA and $L2_1$ structures, distance from the convex hull for the XA phase $\Delta E_{\rm HD}^{XA}$, previous experimental reports.

X_2YZ	a (Å)	$E_g^{\uparrow}$ (eV)	$E_g^{\downarrow}$ (eV)	$m(X_1)$ (μ_B)	$m(X_2)$ (μ_B)	$m(Y)$ (μ_B)	$m(Z)$ (μ_B)	ΔE_f^{XA} (eV/atom)	$\Delta E_f^{L2_1}$ (eV/atom)	$\Delta E_{\rm HD}^{XA}$ (eV/atom)
Sc_2MnP	6.18	0.052	0.052	0	0	0	0	-0.286	-0.471	0.631
Sc_2FeSi	6.255	0.347	0.347	0	0	0	0	-0.292	-0.416	0.311
Sc_2FeGe	6.33	0.356	0.356	0	0	0	0	-0.262	-0.435	0.371
Sc_2FeSn	6.60	0.337	0.337	0	0	0	0	-0.230	-0.358	0.319
Sc_2CoAl	6.42	0.475	0.475	0	0	0	0	-0.280	-0.350	0.130
Sc_2CoGa	6.36	0.532	0.532	0	0	0	0	-0.328	-0.454	0.159
Sc_2CoIn	6.61	0.470	0.470	0	0	0	0	-0.205	-0.281	0.200
Ti_2VSb	6.47	0.427	0.119	-1.236	-0.521	1.881	-0.009	-0.215	-0.208	0.162
Ti_2CrSi	6.11	0.475	0.086	-1.157	-0.787	2.129	-0.036	-0.337	-0.385	0.230
Ti_2CrGe	6.20	0.522	0.104	-1.254	-0.883	2.348	-0.022	-0.262	-0.305	0.259
Ti_2CrSn	6.47	0.579	0.133	-1.396	-1.018	2.727	-0.016	-0.181	-0.154	0.139
Ti_2MnAl	6.23	0.561	0.043	-1.202	-1.067	2.606	-0.043	-0.268	-0.302	0.088
Ti_2MnGa	6.20	0.603	0.034	-1.201	-1.115	2.611	-0.020	-0.287	-0.341	0.114
Ti_2MnIn	6.47	0.394	0.042	-1.336	-1.266	3.043	-0.020	-0.100	-0.05	0.092

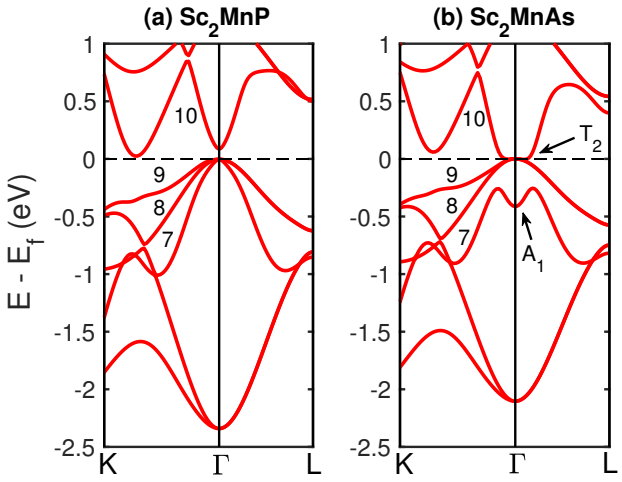

FIG. 12. The band structures of (a) Sc_2MnP and (b) Sc_2MnAs are shown. The singly degenerate A_1 state and triply degenerate T_2 state are labeled in (b). Bands 7, 8, 9 and 10 are labeled in (a) and (b). The zero of the energy axis corresponds to the Fermi level.

magnetic moments and have gaps of different size in the majority and minority spin-channels. The net moment per formula unit is predicted to be zero for the semiconductors, with the Ti moments having the same sign and being balanced by a larger moment of opposite sign on the Y site. If the sign of the moment on the Y atom is taken to be positive, then the larger gaps are in the majority channel while the smaller gaps are in the minority channel, becoming slightly negative for Ti_2VP.

The larger gap (in the majority channel in Table I) for the Ti_2YZ magnetic semiconductors is very similar to the gaps in both channels for the Sc_2YZ non-magnetic semiconductors. The positive moment on the Y atom shifts its majority d-level down while negative moments on the Ti atoms shift their majority d-levels up, the larger moment on the Ti_1 giving it a slightly larger upward shift. As a consequence, the state ordering in the majority channel is Z-s, Z-p, Y-d, Ti_2-d, Ti_1-d so that the majority gap after 9 states per formula unit arises from hybridization between Y-d and X_2-d and X_1-d similar to the case for both channels in the Sc_2YZ 18 electron semiconductors.

The persistence of the very small gaps after 9 states per formula unit in the minority channel is surprising and seems to be aided by avoided band crossings along Γ to K and along L to W. We find these small gaps to be common when the d-levels of the three transition metals are similar. The avoided crossings and hence the gaps are likely symmetry related since the non-magnetic compound V_2VGa has several allowed band crossings that are avoided when the symmetry between X_1, X_2 and Y atoms is broken. These avoided band crossings lead to the small gap after 9 states and are quite common when X_1, X_2 and Y are similar, but not identical in one of the spin channels. For example, simple electron counting ignoring charge transfer and using the calculated moments yields for Ti_2MnGa, that the number of electrons for the minority channel on each atom are approximately 2.6 for X_1 and X_2 and 2.2 for Y. The corresponding minority gap is tiny, 0.034 eV.

The atom-projected DOS of Ti_2CrSn is presented in Fig. 11. The energy ordering of the atomic orbitals is Sn-s (in this case forming a narrow band more than 10 eV below the Fermi level and not shown in the figure.) followed by Sn-p, followed in the majority channel by Cr-d and then the closely spaced Ti_2-d and Ti_1-d. In the minority channel the ordering of the d-states is different, Ti_1-d, Ti_2-d, followed by Cr-d. In the majority channel,

the hybridization between the lower-lying Cr-d and the higher Ti-d states produces a relatively large gap (0.579 eV), while in the minority channel, the relatively closely spaced Cr-d and Ti-d states creates a smaller gap (0.133 eV).

Ti_2CrSn might have interesting spin-dependent transport and tunneling properties if it can be synthesized. The calculated hull distance for the compound is 0.139 eV/atom meaning that the OQMD contains phases or a combination of phases (in this case a mixture of binaries) that is lower in energy than our 0.052 eV/atom empirical threshold.

We found no 24-electron Slater-Pauling semiconductors among the XA compounds that we investigated. Of the 405 XA compounds that we studied, 24 had a valence electron count of 24. None were semiconducting, though 6 were half-metallic with zero moment or near-half-metallic with a very small moment. The reason for the absence of 24-electron XA semiconductors is relatively simple. As we shall discuss in the next section, the Slater-Pauling gap in the XA phase requires formation of significant magnetic moments to create a significant difference between the $d-$onsite energies of the two X atoms. When moments form, the two spin channels will generally be different and a semiconductor becomes unlikely. The interesting exception to this rule are the 18-electron semiconductors with moments, but zero net moment in which even very small differences between the $d-$onsite energies of the X atoms can effectuate a small gap. All of the semiconductors in Table I, have hull distances that exceed our stability threshold criterion of 0.052 eV/atom.

2. *Half-metals and "Near" Half-metals*

Although a large number of XA phase half-metals have been predicted based on theoretical simulations[12], we found that most of them do not remain in the XA phase after relaxation, or they have lower energies in the $L2_1$ or the tetragonal '$L2_1$' phase phase. However, in order to better understand the XA phase, we have listed in Tables II and III all of the half-metals and near-half-metals found in our survey of 405 XA systems for which the calculated formation energy was negative. Our definition of a "near-half-metal" is given in Sec. IV B.

Both tables are divided into three sections according to whether the gap leading to half-metallicity is located after 9, 12 or 14 states. The tables give, N_V, the number of valence electrons per formula unit, a, the lattice constant, the total magnetic moment per formula unit as well as the individual moments on each atom evaluated within atom centered spheres of 1.45 Å radius.

For almost all of the half-metals and near-half-metals that follow the Slater-Pauling rule (gap after 12 states), the spin moments on the X_1 atoms are antiparallel to those on X_2 atoms. If one uses the local moments given in Table II to estimate the number of majority and minority s-d electrons on the transition metal sites one finds that for the Slater-Pauling half-metals with minority gap, there are approximately 4 minority electrons on the X_1 and Y sites and approximately 2 on the X_2 sites. This implies that the transition metal nearest neighbors always differ in number of electrons by approximately 2. The implied contrast in the positions of the d-states of these neighbors leads to the hybridization gap in the minority channel. Since the average of 4 and 2 is 3, the gap should fall after 3 states per atom[73].

The tables also give the formation energy, ΔE_f, and the hull distance calculated within the OQMD, ΔE_{HD} (see Sec IV A 4) as well as the formation energy of the $L2_1$ phase, $E_f(L2_1)$. The final three columns show the calculated energy gap, references to experimental reports of the XA phase and references to experimental reports of the $L2_1$ phase for Y_2XZ. The presence of these phases indicates that it may be difficult to distinguish a mixture of X_2YZ in the XA phase and Y_2XZ in the $L2_1$ phase. Since they have the same XRD reflection peaks, it is difficult to distinguish the composition from the XRD patterns, which may lead to a wrong conclusion about the composition of the sample.

3. *Moment vs. Electron Count*

Figure 13 shows the total spin magnetic moment per formula unit (M_{tot}) plotted versus the total valence electron number per formula unit (N_V) for 254 XA compounds with negative formation energy. In this plot, the half-metallic phases fall along one of the lines, $M_{tot} = |N_V - 18|$, $M_{tot} = |N_V - 24|$, or $M_{tot} = |N_V - 28|$ depending on whether the system is placing the Fermi energy in a gap after 9, 12, or 14 states respectively. The half-metals are listed in Table II along with their calculated properties. Table III is a similar list of the near-half-metals.

The half-metals and near-half-metals found along the $M_{tot} = |N_V - 18|$ line with a gap after 9 states per formula unit in one of the spin channels primarily have X=Sc, or Ti, while those found along the $M_{tot} = |N_V - 24|$ lines generally have X=Cr or Mn. Systems with X=V also fall mainly along the $M_{tot} = |N_V - 18|$ line, but there is one near-half-metal, (V_2CoSi) that uses the gap after 12 states. We find only one half-metal (Mn_2CuSi) and one near-half-metal (Mn_2CuP) along the $M_{tot} = |N_V - 28|$ line. The systems that appear to be on that line at $N_V = 30$ and $N_V = 31$ have pseudogaps rather than gaps near the Fermi energy.

Some systems appear on or near two lines. Systems with $N_V = 21$ can in principle have gaps after both 9 states and 12 states. Ti_2CoSi is a half-metal with the Fermi energy in the minority gap after 9 states, but the Fermi energy also falls in a pseudogap at 12 states in majority. The near-half-metals Ti_2Fe(P,As,Sb) all have gaps after 9 states in minority and after 12 states in majority, however the moment is not large enough to place

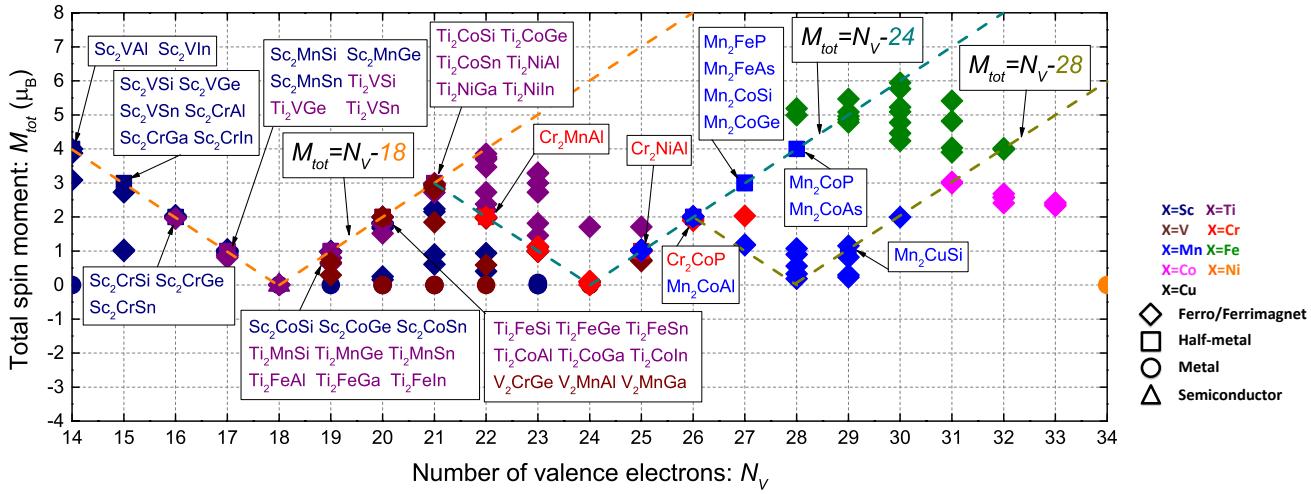

FIG. 13. Calculated total magnetic moment per unit cell as a function of the total valence electron number per unit cell for 254 XA compounds with negative formation energies. The orange dashed line represents $|M_{tot}| = N_V - 18$, the blie dashed line represents the Slater-Pauling rule, $|M_{tot}| = N_V - 24$ and the light green dashed line represents $|M_{tot}| = N_V - 28$. The compounds from Table II are listed in the boxes. All of these compounds follow the rules precisely. We used different colors to label different X-based inverse-Heusler compounds. We used diamond, cubic, circle and triangle symbols to label ferromagnets/ferrimagnets, half-metals, metals and semiconductors, respectively.

the Ferni energy in the gaps. In each case it falls just above the minority gap and just below the majority gap by an equal number of states. Similarly, for $N_V = 26$ one can have systems on both the $M_{tot} = |N_V - 24|$ and the $M_{tot} = |N_V - 28|$ lines. Thus Mn_2CoAl has a minority gap after 12 states and a pseudogap at 14 majority states.

Although we predicted that Mn_2CoSb would have a positive formation energy (0.042 eV), we found references indicating that it can be fabricated in the XA phase [40, 70] using melt-spinning. For this reason Mn_2CoSb was included in Fig. 13 and Table II. As discussed in Sec. III A, we speculate that the experimental samples may be $L2_1B$ phase rather than XA.

4. *Hull Distances*

Using our calculated XA formation energies, and the formation energies of all the other phases in the OQMD, we calculated the hull distance $\Delta E_{\rm HD}$ for the negative formation energy half-metallic inverse-Heusler compounds listed in Table II and the near-half-metals listed in Table III. Our calculations predict all the Sc, Ti-, and V-based half-metals lie significantly above the convex hull and have a $\Delta E_{\rm HD}$ that exceeds our empirical criterion of $\Delta E_{\rm HD} \leq 0.052$eV/atom for having a reasonable probability of synthesizability. We predict 4 half-metals (Cr_2MnAl, Mn_2CoAl, Mn_2CoSi, Mn_2CoGe) to lie close enough to the convex hull to meet our criterion. Two of these compounds Mn_2CoAl[28, 40] and Mn_2CoGe[40] have been experimentally observed by X-ray diffraction (XRD) measurements to exist in the XA phase. We also found 6 near-half-metals (Cr_2MnGa, Mn_2FeAl, Mn_2FeGa, Mn_2FeSi, Mn_2FeGe) that meet our criterion for stability, three of these (Mn_2FeGa, Mn_2FeSi, Mn_2FeGe) have a calculated hull distance of zero meaning that no phase or combination of phases in the OQMD had lower energy.

B. Electronic Structure of each IH Compound

In this section we will briefly discuss each of the 405 XA compounds discussing gaps in their DOS, and whether they are half-metals or near-half-metals. The designation of half-metal is binary. If the Fermi energy lies in a gap for one of the spin-channels, but not for the other, then it is a half-metal. There may be other important quantitative questions such as the distances between the Fermi energy and the band edges, but the calculated band structure either corresponds to a half-metal or it does not. It should be noted that the determination of whether a given inverse-Heusler has a gap is not always trivial if the gap is small because the Brilliouin zone is sampled at a finite number of points. We used both the DOS calculated using the linear tetrahedron method and an examination of the bands along symmetry directions to decide difficult cases.

In contrast to the binary choice between half-metal or not, the designation of a "near-half-metal" is more qualitative. There are a couple of ways a calculated DOS could be "almost" half-metallic; (a) the Fermi energy could fall at an energy for which the DOS for one of the spin chan-

TABLE II. DFT-calculated properties of 51 half-metals in the inverse-Heusler phase that have negative formation energy. Successive columns present: number of valence electrons per formula unit, N_V, calculated lattice constant, a, total spin moment per f.u., M_{tot}, local moments for atoms on the X_1, X_2, Y, and Z sites: $m(X_1)$, $m(X_2)$, $m(Y)$ and $m(Z)$, formation energy ΔE_f, distance from the convex hull ΔE_{HD}, formation energy in $L2_1$ phase $\Delta E_f(L2_1)$, band gap E_g, gap type, experimental reports of compounds with composition X_2YZ, and experimental reports of corresponding Y_2XZ full-Heusler compounds, if any.

X_2YZ	N_V	a (Å)	M_{tot}	$m(X_1)$	$m(X_2)$	$m(Y)$	$m(Z)$ (μ_B)	ΔE_f	ΔE_{HD}	$\Delta E_f(L2_1)$ (eV/atom)	E_g (eV)	Experimental reports	Y_2XZ reports
Sc_2VIn	14	6.938	-4	-0.072	-0.509	-2.675	0.041	-0.013	0.276	-0.100	0.504		
Sc_2VSi	15	6.53	-3	0.058	-0.452	-2.228	0.073	-0.125	0.388	-0.196	0.499		
Sc_2VGe	15	6.61	-3	0.084	-0.424	-2.274	0.070	-0.118	0.446	-0.203	0.480		
Sc_2VSn	15	6.87	-3	0.144	-0.327	-2.388	0.058	-0.157	0.323	-0.210	0.518		
Sc_2CrAl	15	6.67	-3	0.295	-0.064	-3.133	0.082	-0.039	0.225	-0.096	0.684		
Sc_2CrGa	15	6.62	-3	0.284	-0.050	-3.121	0.067	-0.065	0.283	-0.158	0.684		
Sc_2CrIn	15	6.86	-3	0.337	0.056	-3.302	0.049	-0.003	0.286	-0.069	0.646		
Sc_2CrSi	16	6.43	-2	0.380	0.020	-2.454	0.079	-0.120	0.393	-0.161	0.632		
Sc_2CrGe	16	6.52	-2	0.429	0.112	-2.613	0.065	-0.110	0.453	-0.184	0.646		
Sc_2CrSn	16	6.79	-2	0.505	0.234	-2.878	0.051	-0.136	0.344	-0.180	0.631		
Sc_2MnSi	17	6.37	-1	0.465	0.443	-2.218	0.062	-0.200	0.350	-0.285	0.518		
Sc_2MnGe	17	6.461	-1	0.536	0.554	-2.455	0.041	-0.188	0.410	-0.314	0.428		
Sc_2MnSn	17	6.75	-1	0.628	0.654	-2.833	0.031	-0.202	0.312	-0.287	0.266		
Ti_2VSi	17	6.173	-1	0.575	-0.028	-1.476	0.007	-0.316	0.217	-0.379	0.219		
Ti_2VGe	17	6.262	-1	0.688	0.094	-1.706	0.008	-0.246	0.240	-0.316	0.285		
Ti_2VSn	17	6.523	-1	0.879	0.257	-2.052	0.004	-0.166	0.139	-0.189	0.423		
Sc_2CoSi	19	6.28	1	0.426	0.173	0.220	0.053	-0.268	0.406	-0.506	0.67		
Sc_2CoGe	19	6.367	1	0.432	0.221	0.165	0.029	-0.248	0.425	-0.521	0.591		
Sc_2CoSn	19	6.627	1	0.421	0.206	0.182	0.010	-0.239	0.345	-0.421	0.594		
Ti_2MnSi	19	6.024	1	1.055	0.652	-0.920	0.043	-0.394	0.231	-0.409	0.461		
Ti_2MnGe	19	6.123	1	1.204	0.844	-1.314	0.024	-0.295	0.265	-0.346	0.517		
Ti_2MnSn	19	6.39	1	1.41	1.106	-1.916	0.017	-0.188	0.188	-0.178	0.593		
Ti_2FeAl	19	6.12	1	1.013	0.709	-0.964	0.031	-0.256	0.187	-0.279	0.536		
Ti_2FeGa	19	6.122	1	1.005	0.757	-0.966	0.009	-0.265	0.212	-0.344	0.57		
Ti_2FeIn	19	6.37	1	1.208	1.064	-1.673	0.004	-0.045	0.274	-0.072	0.532		
Ti_2FeSi	20	5.99	2	1.257	0.621	-0.101	0.041	-0.395	0.295	-0.447	0.628		
Ti_2FeGe	20	6.07	2	1.282	0.677	-0.186	0.011	-0.297	0.307	-0.394	0.622		
Ti_2FeSn	20	6.339	2	1.356	0.801	-0.509	0.001	-0.185	0.256	-0.227	0.617		
Ti_2CoAl	20	6.13	2	1.252	0.705	-0.204	0.020	-0.287	0.185	-0.293	0.684		
Ti_2CoGa	20	6.11	2	1.230	0.773	-0.211	-0.005	-0.295	0.178	-0.363	0.689		
Ti_2CoIn	20	6.351	2	1.245	0.837	-0.381	-0.009	-0.089	0.195	-0.086	0.613		
V_2CrGe	20	5.94	2	1.167	-0.415	1.158	0.003	-0.118	0.151	-0.120	0.086		
V_2MnAl	20	5.922	2	1.354	-0.309	0.870	0.016	-0.148	0.097	-0.072	0.142		[74]
V_2MnGa	20	5.924	2	1.229	-0.416	1.138	-0.007	-0.118	0.123	-0.070	0.124		[75]
Ti_2CoSi	21	6.02	3	1.528	0.789	0.394	0.059	-0.387	0.307	-0.437	0.798		
Ti_2CoGe	21	6.10	3	1.518	0.812	0.396	0.018	-0.299	0.303	-0.384	0.779		
Ti_2CoSn	21	6.35	3	1.495	0.802	0.373	-0.004	-0.217	0.220	-0.197	0.727		
Ti_2NiAl	21	6.19	3	1.524	0.982	0.149	0.028	-0.285	0.200	-0.277	0.46		
Ti_2NiGa	21	6.17	3	1.491	1.056	0.158	-0.003	-0.289	0.193	-0.364	0.522		
Ti_2NiIn	21	6.4	3	1.452	1.058	0.135	-0.013	-0.127	0.216	-0.096	0.418		
Cr_2MnAl	22	5.831	−2	-1.835	1.536	-1.678	-0.021	-0.086	0.048	0.002	0.204		
Cr_2NiAl	25	5.7	1	-1.239	1.828	0.452	-0.057	-0.071	0.236	0.148	0.142		[76]
Cr_2CoP	26	5.619	2	-0.794	1.912	0.854	-0.012	-0.22	0.217	-0.159	0.48		
Mn_2CoAl	26	5.735	2	-1.617	2.701	0.958	-0.061	-0.27	0.036	-0.141	0.38	XA[28, 40]	[77]
Mn_2FeP	27	5.558	3	-0.452	2.632	0.733	0.024	-0.352	0.096	-0.292	0.252		
Mn_2FeAs	27	5.72	3	-0.732	2.772	0.885	0.022	-0.071	0.086	0.014	0.337		
Mn_2CoSi	27	5.621	3	-0.548	2.670	0.849	-0.012	-0.365	0.018	-0.177	0.513		[78–80]
Mn_2CoGe	27	5.75	3	-0.804	2.863	0.903	0.005	-0.153	0.03	-0.011	0.323	XA[40]	[81]
Mn_2CoP	28	5.581	4	0.091	2.793	1.017	0.032	-0.333	0.216	-0.232	0.508		
Mn_2CoAs	28	5.738	4	-0.007	2.916	1.013	0.025	-0.085	0.08	0.081	0.295		
Mn_2CoSb	28	5.985	4	-0.041	3.093	0.938	-0.003	0.042	0.133	0.193	0.499	XA[40, 70]	[76, 82]
Mn_2CuSi	29	5.762	1	-1.876	2.838	0.003	0.018	-0.101	0.177	-0.091	0.318		

TABLE III. DFT-calculated properties of 50 near-half-metallic X_2YZ inverse-Heusler compounds with negative formation energy. Successive columns present: number of valence electrons per formula unit N_V, calculated lattice constant (a_{calc}), total spin moment (M_{tot}) per f.u., local moments for atoms on the X_1, X_2, Y and Z sites: $m(X_1)$, $m(X_2)$, $m(Y)$ and $m(Z)$, formation energy (ΔE_f), distance from the convex hull ΔE_{HD}, formation energy in $L2_1$ phase $\Delta E_f(L2_1)$, experimental reports of compounds with composition X_2YZ, and experimental reports of corresponding Y_2XZ full-Heusler compounds.

X_2YZ	N_V	a_{calc} (Å)	M_{tot} (μ_B)	$m(X_1)$	$m(X_2)$	$m(Y)$	$m(Z)$	ΔE_f	ΔE_{HD} (eV/atom)	$\Delta E_f(L2_1)$	Experimental records	Rep. Y_2XZ
Sc_2VAl	14	6.756	-3.8779	-0.077	-0.508	-2.588	0.040	-0.033	0.231	-0.134		
Sc_2VGa	14	6.708	-3.9989	-0.114	-0.579	-2.613	0.050	-0.064	0.285	-0.184		
Sc_2MnAl	16	6.59	-1.9983	0.429	0.231	-2.903	0.074	-0.122	0.174	-0.160		
Sc_2MnGa	16	6.54	-1.9999	0.425	0.285	-2.919	0.052	-0.159	0.229	-0.243		
Sc_2MnIn	16	6.80	-1.9969	0.489	0.398	-3.203	0.038	-0.085	0.221	-0.138		
Sc_2VSb	16	6.78	-2.0011	0.319	-0.188	-1.949	0.049	-0.150	0.439	-0.173		
Ti_2VAl	16	6.32	-1.9633	0.380	-0.579	-1.541	0.016	-0.120	0.153	-0.179		
Ti_2VGa	16	6.27	-1.9529	0.314	-0.567	-1.499	0.022	-0.145	0.189	-0.219		
Sc_2CrP	17	6.303	-1.0043	0.491	0.349	-2.051	0.063	-0.166	0.699	-0.296		
Sc_2CrSb	17	6.74	-1.0001	0.660	0.526	-2.598	0.046	-0.097	0.492	-0.178		
Sc_2FeAl	17	6.47	-0.9071	0.248	0.216	-1.539	0.029	-0.1323	0.216	-0.244		
Sc_2FeGa	17	6.43	-0.9488	0.264	0.277	-1.656	0.015	-0.1735	0.267	-0.345		
Sc_2FeIn	17	6.69	-0.9714	0.344	0.412	-2.042	0.013	-0.069	0.290	-0.189		
Ti_2CrAl	17	6.297	-0.8021	1.032	0.775	-2.723	0.019	-0.1556	0.141	-0.197		
Ti_2CrGa	17	6.266	-0.8659	1.008	0.785	-2.747	0.011	-0.1781	0.166	-0.245		
Ti_2CrIn	17	6.51	-0.8538	1.141	0.939	-3.078	0.005	-0.002	0.149	0.022		
Sc_2MnSb	18	6.685	0.0047	-0.656	-0.712	1.984	0.018	-0.1449	0.444	-0.296		
Ti_2VP	18	6.06	0.0033	-0.941	-0.365	1.371	-0.013	-0.4397	0.442	-0.495		
Sc_2NiAl	19	6.502	0.9649	0.413	0.217	0.120	0.031	-0.2413	0.249	-0.425		
Sc_2NiGa	19	6.453	0.9738	0.423	0.272	0.081	0.015	-0.2817	0.278	-0.544		
Sc_2NiIn	19	6.69	0.9839	0.414	0.271	0.078	0.006	-0.1993	0.309	-0.375		
Ti_2CrAs	19	6.11	0.8077	1.015	0.535	-0.941	0.023	-0.2035	0.444	-0.255		
Ti_2CrSb	19	6.38	0.965	1.301	0.775	-1.441	0.019	-0.111	0.279	-0.084		
Sc_2CoSb	20	6.64	1.9999	0.656	0.299	0.664	0.055	-0.138	0.528	-0.394		
Sc_2NiSi	20	6.38	1.8015	0.689	0.459	0.220	0.093	-0.203	0.527	-0.591		
Sc_2NiGe	20	6.46	1.8123	0.691	0.517	0.184	0.050	-0.200	0.540	-0.621		
Sc_2NiSn	20	6.72	1.8438	0.690	0.523	0.164	0.019	-0.228	0.430	-0.516		
Ti_2MnSb	20	6.323	1.9891	1.318	0.564	-0.231	0.009	-0.1596	0.277	-0.181		
Ti_2FeAs	21	6.07	2.9395	1.424	0.469	0.780	0.036	-0.2374	0.475	-0.391		
V_2FeGa	21	5.91	2.8487	1.803	-0.231	1.200	-0.001	-0.146	0.091	-0.047		[76]
Ti_2NiSn	22	6.427	3.8602	1.604	1.307	0.451	0.001	-0.189	0.294	-0.236		
Ti_2FeSb	21	6.31	2.9885	1.449	0.441	0.802	0.009	-0.1583	0.319	-0.209		
V_2FeAl	21	5.914	2.911	1.862	-0.197	1.132	0.026	-0.191	0.088	-0.023		[83]
V_2MnGe	21	5.92	-2.8136	-1.627	0.516	-1.610	0.005	-0.193	0.115	-0.110		
V_2MnSn	21	6.20	-2.9604	-1.690	0.944	-2.148	0.014	-0.002	0.188	0.179		
V_2FeGe	22	5.891	-1.9779	-1.415	0.434	-0.944	-0.004	-0.165	0.146	-0.129		
Cr_2MnGa	22	5.832	-1.993	-1.880	1.614	-1.716	-0.003	-0.004	0.049	0.038		
Cr_2MnGe	23	5.8	-0.9919	-1.478	1.610	- 1.147	0.010	-0.007	0.122	-0.008		
V_2CoSi	23	5.78	-0.997	-0.754	0.182	-0.374	-0.029	-0.291	0.199	-0.193		
Cr_2CoAl	24	5.79	0.0095	1.892	-1.698	-0.307	0.086	-0.08	0.227	0.126		[84]
Cr_2CoSi	25	5.657	1.0086	-0.949	1.440	0.547	0.053	-0.2187	0.139	-0.022		
Cr_2CoGe	25	5.792	1.0225	-1.593	2.034	0.619	0.043	-0.0171	0.109	0.155		
Mn_2FeAl	25	5.75	1.0009	-1.856	2.714	0.142	-0.025	-0.158	0.008	-0.086		[75]
Mn_2FeGa	25	5.79	1.0386	-2.185	2.888	0.315	-0.004	-0.075	0.018	-0.038		
Cr_2NiSi	26	5.705	1.8915	-0.857	2.130	0.573	-0.023	-0.195	0.201	-0.035		
Cr_2NiGe	26	5.82	1.9414	-1.132	2.434	0.573	-0.008	-0.012	0.176	0.124		
Mn_2CoGa	26	5.76	2.0045	-1.820	2.879	0.955	-0.030	-0.167	0	-0.087	XA[40]	[85]
Mn_2FeSi	26	5.6006	2.0077	-0.798	2.407	0.371	-0.015	-0.362	0	-0.259		[76]
Mn_2FeGe	26	5.72	2.0135	-1.243	2.667	0.556	-0.004	-0.14	0	-0.035		
Mn_2CuP	30	5.716	1.9946	-1.242	3.042	0.057	0.083	-0.048	0.399	-0.091		

nels is very small, i.e. a pseudogap, (b) the DOS could have a gap in one of the spin channels with the Fermi energy lying slightly outside the gap. If we choose criterion (a) we must choose a threshold for "very small" and if we choose (b) we must choose a threshold for "slightly". Criterion (a) is difficult to implement because there are an infinite number of ways the DOS can vary near a pseudogap, e.g. a pseudogap may be wide and only fairly small or it might be narrow but extremely small or some combination. Another issue with criterion (a) is that a low density of states is often associated with a highly dispersive band that leads to a large conductivity. For these reasons, we choose criterion (b), i.e. we require that there be an actual gap and that the Fermi energy fall "near" this gap. The (arbitrary) criterion we choose for "near" is 0.2 electron states per formula unit. Other criteria could be used, e.g. the distance from the Fermi energy to the nearest band edge. Our choice of using the number of states has the advantage of being easily related to the magnetic moment. It has the disadvantage that occasionally a system with a highly dispersive band above or below the Fermi energy with a very small density of states can lead to a situation in which we label a system near-half-metallic when the Fermi energy is as much as 0.3 eV into the band.

For each of the systems, we note the gaps in the DOS, typically after 9, 12 or 14 states per formula unit per spin channel and whether the Fermi energy falls in one or more of the gaps or close enough to the gap (0.2 states) to be designated a near-half-metal. Simple state and electron counting dictates that to make a half-metal by taking advantage of a gap after N_s states when there are N electrons per formula unit, the magnetic moment per formula unit must be $N - 2N_s$.

13 electron systems: Our dataset contained 3 systems with 13 valence electrons, Sc_2Ti(Al,Ga,In). All three were magnetic metals with small gaps after 9 states per spin channel in both channels (except for Sc_2TiIn minority). However, the moments were not large enough (a total moment of 5 μ_B per formula unit would have been needed) to move the majority Fermi energy into the gap.

14 electrons systems: Our dataset contained 6 systems with 14 valence electrons, Sc_2Ti(Si,Ge,Sn) and Sc_2V(Al,Ga,In). These systems require a moment of 4 μ_B to place the Fermi energy in a majority gap after 9 electrons per spin channel.

Sc_2Ti(Si,Ge,Sn): Sc_2TiSi and Sc_2TiGe are predicted to be non-magnetic metals and to have small gaps after 9 states in both spin channels. Sc_2TiSn is predicted to be magnetic and to have a majority gap after 9 states, but its moment closer to 3 than 4 μ_B.

Sc_2V(Al,Ga,In): These all have relatively large gaps after 9 states in the majority channel. The position of the Fermi energy rises relative to the gap as the atomic size of the Z atom increases the lattice constant, facilitating the formation of large moments on V and even small moments on Sc. For Sc_2VAl and Sc_2VGa, the moment is not quite large enough to place the Fermi energy in the gap making them near-half-metals (Table III). However, the lattice constant of Sc_2VIn *is* large enough to support a moment large enough to move the Fermi energy into the gap so it is a half-metal (Table II).

15 electron systems: Our dataset contained 9 systems with 15 valence electrons, Sc_2Ti(P,As,Sb), Sc_2V(Si,Ge,Sn) and Sc_2Cr(Al,Ga,In). A moment of 3 μ_B is needed to place the Fermi energy in a majority gap after 9 states.

Sc_2Ti(P,As,Sb): These systems do not have gaps after 9 states per atom in either channel because of a reordering of the states at Γ. A singly degenerate state, usually band 10 at Γ, interchanges with a triply degenerate T_2 state so that bands 8, 9, and 10 are associated with the triply degenerate T_2 state, precluding a gap.

Sc_2V(Si,Ge,Sn): These systems have majority gaps after 9 states. The Fermi energy is in the gap and they are classified as half-metals as described in Table II.

Sc_2Cr(Al,Ga,In): These systems all have large gaps after 9 states in majority and small gaps or pseudogaps near 9 states in minority. The Fermi energy falls in the majority gap for all three so they are classified as half-metals and described in Table II.

16 electron systems: Our dataset contained 12 systems with 16 valence electrons per formula unit, Sc_2V(P,As,Sb), Sc_2Cr(Si,Ge,Sn), Sc_2Mn(Al,Ga,In), and Ti_2V(Al,Ga,In). For 16 valence electrons per formula unit and a gap after 9 states in the majority spin channel, a moment of 2 μ_B is needed to place the Fermi energy in the gap to make a half-metal.

Sc_2V(P,As,Sb): Sc_2VP and Sc_2VAs have a region with an extremely low but non-zero DOS at the Fermi energy. These pseudogaps can be be traced to a band reordering similar to that mentioned previously in which a singly degenerate state at Γ drops below a triply degenerate state so that the triply degenerate state connects to bands 8, 9 and 10, thus precluding a gap. In the case of Sc_2VSb, the singly degenerate state is a few hundredths of an eV above the triply degenerate state so it is a near-half-metal with a tiny gap.

Sc_2Cr(Si,Ge,Sn): These systems have large majority gaps after 9 states. They generated half-metals as described in Table II.

Sc_2Mn(Al,Ga,In): The three systems with X=Sc and Y=Mn have large majority and tiny minority gaps after 9 states. Their moments are very slightly less than 2 μ_B so they generated near-half-metals as described in Table III by placing the Fermi energy at the valence edge of the majority gap.

Ti_2V(Al,Ga,In): These systems have tiny majority and minority gaps after 9 states per spin channel. All take advantage of the majority gap to generate near-half-metals as shown in Table III. Ti_2VIn is not included in the table because it has a positive formation energy.

17 electron systems: Our dataset contained 15 systems that had 17 electrons per formula unit, Sc_2Cr(P,As,Sb), Sc_2Mn(Si,Ge,Sn), Sc_2Fe(Al,Ga,In), Ti_2V(Si,Ge,Sn), and Ti_2Cr(Al,Ga,In). Systems with 17

electrons per formula unit can generate half-metals by taking advantage of a gap after 9 states in majority if their magnetic moment per formula unit is 1 μ_B.

Sc_2Cr(P,As,Sb): Sc_2CrP and Sc_2CrAs both have majority pseudogaps at the Fermi energy. The gap after 9 electrons per formula unit is converted into a pseudogap by a band reordering at Γ similar to that occurring for Sc_2V(P,As) and Sc_2Ti(P,As,Sb). Sc_2CrSb has a "normal" band ordering at Γ and is a near-half-metal similar to Sc_2VSb, but with a much larger gap.

Sc_2Mn(Si,Ge,Sn): These systems have majority gaps after 9 states and are all half-metals as described in Table II. In addition to the majority gap Sc_2MnSi has a gap after 9 states in minority. A pseudogap near 9 states in minority for Sc_2MnSi can also be identified.

Sc_2Fe(Al,Ga,In): These systems have gaps after 9 states in both majority and minority channels. All three take advantage of the majority gap to generate near-half-metals as described in Table III. Sc_2FeAl also has a minority pseudogap near 12 states and a majority pseudogap near 14 states.

Ti_2V(Si,Ge,Sn): These all have gaps after 9 states in both majority and minority with the majority gap being larger. All three compounds utilize the majority gap to form half-metals as described in Table II.

Ti_2Cr(Al,Ga,In): These have gaps after 9 states in both spin channels. They are all near-half-metals (Table III), having moments just large enough to satisfy our criterion. The large moment on the Cr atom opens a large gap in the majority channel (hybridization between Cr and Ti-*d* and with the Cr *d*-onsite energy well below that of the Ti atoms). The gap in minority is smaller and is dependent on the difference between the two Ti potentials and avoided band crossings.

18 electron systems: Our dataset contained 18 systems with 18 valence electrons. These were described in Section IV A 1.

19 electron systems: Our dataset contained 21 systems with 19 valence electrons per formula unit, Sc_2Fe(P,As,Sb), Sc_2Co(Si,Ge,Sn), Sc_2Ni(Al,Ga,In), Ti_2Cr(P,As,Sb), Ti_2Mn(Si,Ge,Sn), Ti_2Fe(Al,Ga,In), and V_2Cr(Al,Ga,In). Systems with 19 valence electrons need a moment of 1 μ_B to place the Fermi energy in a gap after 9 states in the minority channel.

Sc_2Fe(P,As,Sb): Sc_2FeP is non-magnetic with gaps after 9 states in both spin channels. Sc_2FeAs is also non-magnetic, but the gaps after 9 states are converted to pseudogaps by the inversion of singly and triply degenerate states at Γ similar to Sc_2CrP and Sc_2CrAs. The larger lattice constant of Sc_2FeSb allows it to develop a moment. There are sizeable gaps after 9 states in both the minority and majority channels, but the moment is not quite large enough (0.79 μ_B) to meet our criterion for calling it a near-half-metal.

Sc_2Co(Si,Ge,Sn): All three of these are half-metals with sizable gaps after 9 states in both spin channels (Table III). The Fermi energy falls near the top of the gap, in all three cases but especially for Ge.

Sc_2Ni(Al,Ga,In): All three have sizable gaps after 9 states in both spin channels and moments as given in Table III that qualify them as near-half-metals.

Ti_2Cr(P,As,Sb): All three compounds have gaps in the minority channel after 9 states, but only and Ti_2CrAs and Ti_2CrSb have sufficiently large moments to be classified as near-half-metals. (Ti_2CrAs only barely made the cut-off.) Ti_2CrSb also has a tiny gap after 9 states in majority.

Ti_2Mn(Si,Ge,Sn): All three of these compounds have sizable gaps after 9 states in minority and much smaller gaps in majority. They also have pseudogaps near 12 states in minority. For all three, the Fermi energy falls in the gap so they are are included in Table III.

Ti_2Fe(Al,Ga,In): All three of these compounds have gaps after 9 states in both channels and peseudogaps in both channels after 12 states. The gaps after 9 states are much smaller in majority than in minority. The Fermi energy for each of the three falls in the minority gap creating three half-metals as described in Table II.

V_2Cr(Al,Ga,In): All three of these systems have gaps after 9 states in both spin channels. In all cases, however, the magnetic moment is not large enough to meet our criterion for a near-half-metal. The formation energy is small and negative for V_2CrAl and V_2CrGa. It is positive for V_2CrIn.

20 electron systems: Our dataset contained 24 compounds with 20 electrons per formula unit, Sc_2Co(P, As, Sb), Sc_2Ni(Si, Ge, Sn), Sc_2Cu(Al, Ga, In), Ti_2Mn(P, As, Sb), Ti_2Fe(Si, Ge, Sn), Ti_2Co(Al,Ga,As), V_2Cr(Si, Ge, Sn) and V_2Mn(Al, Ga, In).

Sc_2Co(P,As,Sb): Sc_2CoP and Sc_2CoAs both have gaps after 9 states per formula unit in both spin channels, but in both cases the net magnetic moment is much too small to pull the Fermi energy into one of the gaps. Sc_2CoSb, on the other hand, due to its larger lattice constant supports a moment sufficiently large (1.999 μ_B) that the Fermi energy falls at the top edge of the minority gap. We classify it as a near-half-metal (Table III).

Sc_2Ni(Si,Ge,Sn): The compounds, Sc_2Ni(Si,Ge,Sn), all have gaps after 9 electrons in both spin channels. However, the total moment (1.80 μ_B, 1.81 μ_B, 1.84 μ_B respectively) does not reach the value (2.00 μ_B) needed to place the Fermi energy in the gap. Even when the lattice is expanded the magnetic moment of these Sc_2Ni(Si,Ge,Sn) compounds hardly increases because the d-bands of Ni are filled so that Ni only supports a very small moment in these materials. Nevertheless, these compounds meet (barely) our threshold to be called near-half-metals (Table III).

Sc_2Cu(Al,Ga,In): The systems Sc_2Cu(Al,Ga,In) all have pseudogaps after 9 states in both spin channels.

Ti_2Mn(P,As,Sb):All three of these compounds have gaps after 9 electrons in both spin-channels. However only Ti_2MnSb (due to its larger lattice constant) has a moment (1.989 μ_B) close enough to 2 μ_B to be classified a "near-half-metal". Ti_2MnAs (1.7967 μ_B) barely misses the cut-off to be included in Table III.

Ti_2Fe(Si, Ge, Sn): The compounds Ti_2Fe(Si,Ge,Sn) all have gaps in both channels after 9 states and pseudogaps after 12 states. The Fermi energy falls within the gap in all three cases so they are predicted to be half-metals as described in Table II.

Ti_2Co(Al,Ga,As): The compounds Ti_2Co(Al,Ga,In) have large minority gaps after 9 states and somewhat smaller gaps after 9 states in majority. The Fermi energy falls within the minority gap in all three cases so they are are predicted to be half-metals as described in Table II.

V_2Cr(Si,Ge,Sn):V_2CrSi has small gaps after 9 states in both spin channels, but is not magnetic. V_2CrGe is magnetic with a moment of 2 μ_B. The Fermi energy falls very close to the top of the gap, but V_2CrGe is predicted to be a half-metal as described in Table II. V_2CrSn has a gap after 9 states in the majority channel which is not useful for generating a half-metal. There is no gap in minority.

V_2Mn(Al, Ga, In): V_2MnAl has a tiny majority gap and a sizable minority gap after 9 states. It also has pseudogaps after 12 states in majority and 14 states in minority. It takes advantage of the minority gap after 9 states to become a half-metal. The DOS for V_2MnGa is similar. It is also a half-metal. Both compounds are included in Table II. V_2MnIn has a gap after 9 states in the majority, but only a pseudogap after 9 states in minority. Its large moment, in excess of $3\mu_B$, places the Fermi energy well below this pseudogap.

21 electron systems: Our database contains 27 systems with 21 valence electrons, Sc_2Ni(P,As,Sb), Sc_2Cu(Si,Ge,Sn), Sc_2Zn(Al,Ga,In), Ti_2Fe(P,As,Sb), Ti_2Co(Si,Ge,Sn), Ti_2Ni(Al,Ga,In), V_2Cr(P,As,Sb), V_2Mn(Si,Ge,Sn), V_2Fe(Al,Ga,In). Systems with 21 valence electrons are interesting because they can, in principle, place the Fermi energy in a gap after 9 electrons or a gap after 12 electrons or both. If a majority gap present after 12 states is present as well as a minority gap after 9 states, a moment of 3 μ_B would yield a magnetic semiconductor.

Sc_2Ni(P,As,Sb): Sc_2NiP has tiny gaps in both spin channels after 9 states while Sc_2NiAs has pseudogaps after 9 states in both spin channels. Both have very small moments. Sc_2NiSb has gaps after 9 states in both spin channels, but its moment (2.15 μ_B) is too small to place the Fermi energy in or near the gap.

Sc_2Cu(Si,Ge,Sn): All three of these compounds have gaps after 9 states in minority and much smaller gaps in majorty. However their moments are too small to place the Fermi energy in the minority gap.

Sc_2Zn(Al,Ga,In): These three non-magnetic compounds only have pseudogaps after 9 states in both spin channels because of a highly dispersive band 10 which drops below band 9 along Γ to X.

None of the 21-electron systems with X=Sc generate half-metals or near-half-metals because a moment of 3 μ_B would be necessary to take advantage of a gap after 9 states per spin per formula unit or to take advantage of a gap after 12 states per spin per formula unit. The compounds are not able to do this because Sc is difficult to polarize and Ni, Cu and Zn cannot support a large moment because their d-bands are filled or (in the case of Ni) nearly filled.

Ti_2Fe(P,As,Sb): These three compounds have large gaps after 9 states in the minority channel and smaller gaps in the majority channel after 9 states. Ti_2FeP and Ti_2FeAs have pseudogaps after 12 states in the maority which becomes a very small real gap for Ti_2FeSb. The moments for the three are $2.72\mu_B$, $2.94\mu_B$ and $2.99\mu_B$ respectively. Ti_2FeAs and Ti_2FeSb meet our criterion for near-half-metallicity. If the moment for Ti_2FeSb were very slightly larger, we would predict it to be a magnetic semiconductor with a large minority gap and a tiny majority gap, i.e. a 9/12 magnetic semiconductor. The present prediction is for a magnetic semi-metal that has a pocket of down-spin electrons along Γ to K and a Γ-centered pocket of up-spin holes.

Ti_2Co(Si,Ge,Sn): These three compounds all have gaps in both spin channels after 9 states, with the minority gap being larger. Ti_2CoSi also has a majority pseudogap after 12 states. For all three, the Fermi energy falls within the minority gap giving each a moment of 3 μ_B and making them half-metals (Table II). For Ti_2CoSi the current at zero K would be carried by up-spin holes at Γ and up-spin electrons at X.

Ti_2Ni(Al,Ga,In): These three compounds all have gaps after 9 states in both spin channels. The Fermi energy falls well inside the minority gaps yielding half-metals with moments of 3 μ_B in each case (Table II).

V_2Cr(P,As,Sb): V_2CrP has gaps after 9 states in both spin channels, but is non-magnetic. V_2CrP has a gap in the minority channel after 9 states and a pseudogap after 9 states in the majority channel. Its moment is too small (1.85 μ_B) for it to be classified as a near-half-metal. V_2CrSb has a pseudogap after 9 states in the majority channel and a sizable gap after 12 states also in majority chanel. Its moment is large enough (2.89 μ_B) that we would classify it as a near-half-metal. However, its formation energy is positive so it is not included in Table III.

V_2Mn(Si,Ge,Sn): V_2MnSi has pseudogaps after 9 states in both spin channels and is non-magnetic. V_2MnGe has gaps after 9 states in both spin channels and a pseudogap after 12 states in majority. Its moment of 2.81 μ_B qualifies it (barely) for inclusion with the near-half-metals in Table III. V_2MnSn has majority gaps after 9 and 12 states and a pseudogap after 9 states in minority. It's moment of 2.96 μ_B qualifies it for inclusion in Table III as a Slater-Pauling near-half-metal.

V_2Fe(Al,Ga,In): V_2FeAl has gaps after 9 and 14 states in minority and after 12 states in majority. Its moment of 2.91 μ_B qualifies it as a "double near-half-metal" since its Fermi energy is near gaps after 9 states in minority and 12 states in majority. V_2FeGa has a gap after 9 states in minority and a pseudogap after 12 states in majority. Its moment of 2.85 μ_B meets the threshold for

inclusion in Table III as a near-half-metal. V_2FeIn has gaps in both spin channels after 9 states and a pseudogap after 12 states in majority. Its moment is large enough for inclusion for inclusion in Table III, but its formation energy is positive.

22 electron systems: Our database contains 27 systems with 22 electrons, Sc_2Cu(P,As,Sb), Sc_2Zn(Si,Ge,Sn), Ti_2Co(P,As,Sb), Ti_2Ni(Si,Ge,Sn), Ti_2Cu(Al,Ga,In), V_2Mn(P,As,Sb), V_2Fe(Si,Ge,Sn), V_2Co(Al,Ga,As), and Cr_2Mn(Al,Ga,In). These systems would need a moment of 4 μ_B to place the Fermi energy into a gap after 9 states in the minority channel or a moment of 2 μ_B to place the Fermi energy into a gap after 12 states in the majority channel.

Sc_2Cu(P,As,Sb): The systems with X=Sc and Y=Cu generate only small moments (0.40, 0.62 and 0.79)μ_B for Z=P, As, and Sb respectively. They have gaps in both channels after 9 states and no gaps after 12 states.

Sc_2Zn(Si,Ge,Sn): The systems with X=Sc and Y=Zn also generate moments that are too small (0.55, 0.92 and 0.93 μ_B for Si, Ge, and Sn respectively). These systems have pseudogaps after 9 states in both spin channels, but no gaps after 12 states.

Ti_2Co(P,As,Sb): These three systems have gaps after 9 states in both spin channels, but their moments (2.20, 2.38, and 2.73)μ_B are much smaller than the 4 μ_B needed to place the Fermi energy in the minority gap.

Ti_2Ni(Si,Ge,Sn): These three systems have gaps after 9 states in both spin channels. Their moments are larger than those of the Ti_2Co(P,As,Sb) systems (3.47, 3.69 and 3.86μ_B) for Si, Ge and Sn respectively. Thus, Ti_2NiSn meets our threshold for inclusion in Table III as a near-half-metal.

Ti_2Cu(Al,Ga,In): Ti_2CuAl has gaps after 9 states in both spin channels, but its moment is too low (3.72 μ_B) to meet our criterion for near-half-metal status. Ti_2CuGa and Ti_2CuIn have gaps after 9 states in majority, but only pseduogaps after 9 states in minority.

The 22 electron systems with X=Ti and Y=Co, Ni or Cu tend to have gaps after 9 states per spin channel per formula unit in both spin channels. They do not have gaps after 12 states per spin channel, presumably because insufficient contrast can be generated between the d-onsite energies of the two Ti atoms. In most cases the moments are too small to place the Fermi energy in the minority gap after 9 states. The moments are largely on the Ti atoms and the moments tend to increase with the atomic number of the Y atom, increasing from Co to Ni to Cu, and with the size of the Z atom.

V_2Mn(P,As,Sb): V_2MnP has gaps after 9 states in both spin channels but a very small moment (0.59 μ_B) so it cannot take advantage of the minority gap to make a half-metal. V_2MnAs also has gaps after 9 states in both channels and a pseudogap after 12 states in the majority. Its moment of 1.97 μ_B places the Fermi energy close to the majority pseudogap after 12 states, but the absence of a real gap precludes its designation as a near-half-metal. V_2MnSb has a majority gap after 9 states, a minority pseudogap after 9 states and a majority gap after 12 states. Its moment of 1.9987 μ_B places the Fermi energy just below the majority gap after 12 states. Only its positive formation energy precludes its inclusion in Table III.

V_2Fe(Si,Ge,Sn): All three compounds have gaps after 9 states in both spin channels. V_2FeGe also has a majority gap after 12 states and V_2FeSn has a pseudogap after 12 states in the majority channel. The moment of V_2FeGe (1.98 μ_B) places its Fermi energy quite close to the majority gap so it is a near-half-metal as described in Table III.

V_2Co(Al,Ga,As): All three of these compounds have gaps in both channels after 9 states with the minority gap being much larger than the small majority gap. All three also have pseudogaps after 12 states in the majority. The pseudogap for V_2CoAl is particularly pronounced. The moment is slightly less than 2 μ_B for all three compounds, but according to our definition, they are not near-half-metals.

Cr_2Mn(Al,Ga,In):Cr_2MnAl and Cr_2MnGa both have gaps after 12 states in the majority channel. Cr_2MnIn only has a pseudogap there. Cr_2MnAl is a half-metal as described in Table II and Cr_2MnGa is a near-half-metal as described in Table III. All three of these compounds are predicted to have ferrimagnetic states in which the moments of Cr_1 and Mn are aligned, and the moment of Cr_2 is opposite.

23 electron systems: Our database contains 27 systems with 23 electrons, Sc_2Zn(P,As,Sb), Ti_2Ni(P,As,Sb), Ti_2Cu(Si,Ge,Sn), Ti_2Zn(Al,Ga,In), V_2Fe(P,As,Sb), V_2Co(Si,Ge,Sn), V_2Ni(Al,Ga,In), Cr_2Mn(Si,Ge,Sn), and Cr_2Fe(Al,Ga,In). These compounds can take advantage of a gap after 9 states in minority to make a half-metal, but a moment of 5 μ_B would be needed. Alternatively, they could take advantage of a gap after 12 states in majority which would only require a moment of 1 μ_B. A few of these systems have pseudogaps after 14 states. In principle, one could have a 23 electron inverse-Heusler magnetic semiconductor with a moment of 5 μ_B that uses gaps after 9 states in minority and 14 states in majority; however such solutions did not appear in our database.

Sc_2Zn(P,As,Sb): The three systems Sc_2Zn(P,As,Sb) have pseudogaps after 9 states in both channels. They are all non-magnetic and have no gaps after 12 sates.

Ti_2Ni(P,As,Sb): These compounds all have gaps after 9 states in both spin-channels, but their moments are much too small to make half-metals or near-half-metals.

Ti_2Cu(Si,Ge,Sn): The three systems Ti_2Cu(Si,Ge,Sn) have gaps in both channels after 9 and pseudogaps in majority after 14 states. Their moments, however (3.00, 3.16, and 3.33)μ_B are much less than the 5 μ_B that would be needed to place the Fermi energy in the minority gap.

Ti_2Zn(Al,Ga,In): These compounds all have pseudogaps near 9 states per formula unit in the minority channel but no gaps at 9 or 12 states nor is the Fermi energy near the pseudogap. Ti_2ZnAl and Ti_2ZnGa also

have majority gaps after 9 states and Ti_2ZnAl also has a pseudogap after 14 states in majority.

V_2Fe(P,As,Sb): These compounds have gaps in both spin channels after 9 states. V_2FeP and V_2FeAs have pseudogaps in the majority channel after 12 states. V_2FeSb, however does have a majority gap after 12 states and the magnetic moment (0.9996 μ_B) places the Fermi energy at the lower edge of this gap. V_2FeSb is not included in Table III because it has a positive formation energy.

V_2Co(Si,Ge,Sn): These compounds have gaps after 9 states in both channels, but only pseudogaps after 12 states except for V_2CoSi which has a tiny gap after 12 states. The Fermi energy falls just below this gap (moment = 0.997 μ_B). (See Table III.)

V_2Ni(Al,Ga,In): These compounds have sizable gaps after 9 states in both spin channels, but the moments are small ($\approx 1\mu_B$) and there are no gaps after 12 states in the majority channel, hence no half-metals or near-half-metals.

Cr_2Mn(Si,Ge,Sn): Cr_2MnSi has a gap after 9 states in the majority channel and a pseudogap after 9 states in minority. Cr_2MnGe has a pseudogap after 9 states in majority and a sizable gap after 12 states in majority. Its moment of 0.99 μ_B allows it to use this gap to become a near-half-metal (Table III). Cr_2MnSn also has a majority gap after 12 states and a moment of approximately 1.00 μ_B so it is a near-half-metal, but it is not included in Table III because its formation energy is positive.

Cr_2Fe(Al,Ga,In): Cr_2FeAl has minority gaps after 9 states and 14 states, and a majority pseudogap near 12 states. Its moment of approximately 1.00 μ_B places the Fermi energy into this peseudogap. Cr_2FeGa has a minority pseudogap after 9 states and a majority gap after 12 states. Its moment of 0.98 μ_B makes it a near-half-metal, but it is not included in Table III because its formation energy is positive. Cr_2FeGa has a majority pseudogap near 12 states.

24 electron systems: Our database contained 24 systems with 24 valence electrons, Ti_2Cu(P,As,Sb), Ti_2Zn(Si,Ge,Sn), V_2Co(P,As,Sb), V_2Ni(Si,Ge,Sn), V_2Cu(Al,Ga,In), Cr_2(P,As,Sb), Cr_2Fe(Si,Ge,Sn), Cr_2Co(Al,Ga,In). Based on electron count alone, these systems would offer the opportunity for non-magnetic semiconductors or zero net moment half-metals arising from Slater-Pauling gaps after 12 states per formula unit in one or both spin-channels. In practice, we find that only four of the 24 systems display Slater-Pauling gaps (and only in one spin-channel). In all four of these systems the Fermi energy falls at the edge of the gap but just outside so that they would be classified as near-half-metals. Three of these four near-half-metals have positive formation energy.

The gaps after 9 states, on the other hand, seem to be more robust. Only Cr_2MnSb failed to show a gap or a pseudogap after 9 states in at least one of the spin channels. Most systems showed gaps after 9 states in both spin channels. However, none of the systems were able to generate a moment of 6 μ_B that would have been necessary to use one of the gaps after 9 states to generate a half-metal.

Ti_2Cu(P,As,Sb): These systems showed gaps in both channels after 9 states, but their moments were much too small to place the Fermi energy near the minority gap.

Ti_2Zn(Si,Ge,Sn): These systems showed pseudogaps in both channels near 9 states per formula unit. The gaps were converted to pseudopgaps by a highly dispersive band 10 along Γ to X dropping down below the maximum of bands 7-9 at Γ.

The 9 systems in our database with X=V all showed gaps after 9 states in both spin channels. In all cases, the moments were quite small so that the Fermi energy could not fall into these gaps. Six of the 9 systems, V_2Co(P,As,Sb) and V_2Ni(Si,Ge,Sn) have pseudogaps around 12 states per atom in at least one spin channel.

V_2Co(P,As,Sb): These systems show gaps after 9 states and pseudogaps after 12 states in both spin channels. The moments are too small (V_2CoSb) or zero precluding half-metals.

V_2Ni(Si,Ge,Sn): V_2NiSi has gaps in both spin channels after 9 states and pseudogaps after both spin channels after 12 states. V_2NiGe has gaps in both spin channels after 9 states and a marginal pseudogap after 12 states in majority. V_2NiSn has gaps after 9 states in both spin channels and pseudogaps after 12 states in minority and after 14 states in majority. The lack of real gaps after 12 states and their very small moments preclude half-metals.

V_2Cu(Al,Ga,In): These compounds have gaps after 9 states in both spin channels and minority gaps after 14 states. V_2CuIn also has a majority gap after 14 states while V_2CuAl and V_2CuGa have pseudogaps in majority near 14 states. Their small moments and the absence of gaps after 12 states preclude half-metals.

Cr_2Mn(P,As,Sb): In the minority channel, Cr_2MnP has a gap after 9 states and a pseudogap near 12 states. It also has a pseudogap near 9 states in majority. It has a small moment placing the Fermi energy in the minority pseudogap near 12 states. Cr_2MnAs has minority gaps after 9 and 12 states. The very small moment (0.005 μ_B)places the Fermi energy just below the gap at 12 states. Thus Cr_2MnAs is a near-half-metal, but it is not included in Table III because its calculated formation energy is positive. Cr_2MnSb has a minority gap after 12 states. Its tiny moment (0.0002 μ_B) makes it a near-half-metal, but it is not included in Table III because its formation energy is positive.

Cr_2Fe(Si,Ge,Sn): Cr_2FeSi is non-magnetic and has gaps after 9 states in both channels. Cr_2FeGe has gaps in both spin channels after 9 states and a minority gap after 12 states. Its small moment makes it a near-half-metal, but we do not list it in Table III because of its positive formation energy. Cr_2FeSn has a majority gap after 9 states and a minority gap after 12 states. Its small moment places the Fermi energy somewhat below this gap yielding a near-half-metal. It is not listed in Table III

because of its positive formation energy.

Cr_2Co(Al,Ga,In): These systems all have gaps after nine states in the majority channel and all have gaps (Al,Ga) or pseudogaps (In) in the minority channel after 12 states. All three have tiny moments. Cr_2CoAl and Cr_2CoGa are near-half-metals, but only the former has a negative formation energy. Cr_2CoAl is the only Slater-Pauling 24 electron near-half-metal with negative formation energy in Table III.

25 electron systems: Ti_2Zn(P,As,Sb), V_2Ni(P,As,Sb), V_2Cu(Si,Ge,Sn) V_2Zn(Al,Ga,In), Cr_2Fe(P,As,Sb), Cr_2Co(Si,Ge,Sn), Cr_2Ni(Al,Ga,As), Mn_2Fe(Al,Ga,As). Many of the 25 electron inverse-Heusler systems show gaps after 9 states per formula in one or both spin-channels. None of these systems, however, are able to take advantage of these gaps to make a half-metal or near-half-metal by moving the Fermi energy to the gap, because that would require a relatively large moment (7 μ_B per formula unit). This large moment would be difficult to produce in systems whose transition metal elements come from the early or late part of the transition metal series, e.g. X=Ti or V and Y=Ni, Cu or Zn. The systems that could produce such large moments, e.g. X=Cr or Mn and Y=Fe or Co seem to prefer smaller net moments closer to 1 μ_B which allows them to take advantage of gaps and pseudogaps after 12 states per formula unit. Several systems show gaps after 14 states, but none of these have the correct moment (3 μ_B) to make a half-metal.

Ti_2Zn(P,As,Sb): All three compounds have gaps after 9 states in both spin channels, but their moments are too small to move the Fermi energy near these gaps.

V_2Ni(P,As,Sb): All three compounds have gaps after 9 states in both spin channels, but their moments are too small to move the Fermi energy near these gaps.

V_2Cu(Si,Ge,Sn): All three compounds have gaps after 9 states in both spin channels. V_2CuSn also has gaps after 14 electrons in both spin channels. In all three cases, the moments are too small to move the Fermi energy near the minority gap after 9 states or the majority gap after 14 states.

V_2Zn(Al,Ga,Sb): V_2ZnAl has a gap after 14 states in majority and a pseudogap after 14 states in minority. V_2ZnGa has a pseudogap after 14 states in majority and a gap after 14 states in minority. V_2ZnIn has a gap in both spin channels after 14 states. Their small moments preclude half-metals or near-half-metals.

Cr_2Fe(P,As,Sb): Cr_2FeP has gaps in both spin channels after 9 states and a pseudogap in minority after 12 states. Cr_2FeAs has gaps in both spin channels after 9 states and a sizable gap in minority after 12 states. Cr_2FeSb has a gap after 9 states in majority and a pseudogap after 9 states in minority. It also has a gap after 12 states in minority. All three have moments of approximately 1.01 μ_B which places the Fermi energy near the gap or pseudogap at 12 states. Cr_2FeAs and Cr_2FeSb are near-half-metals, but are not included in Table III because of their positive formation energies.

Cr_2Co(Si,Ge,Sn): Cr_2CoSi has gaps in both spin channels after 9 states and a minority gap after 12. Cr_2CoGe has a majority gap after 9 states and a minority gap after 12 states. Both of these systems are predicted to be near-half-metals as described in Table III. Cr_2CoSn has a majority gap after 9 states and a pseudogap in minority near 12 states.

Cr_2Ni(Al,Ga,In): Cr_2NiAl has gaps after 9 and 14 states in majority and after 12 states in minority. It uses the gap after 12 states in minority to generate a half-metal as described in Table II. Cr_2NiGa has gaps after 9 states in majority and after 14 states in minority. It also has a pseudogap near 12 states in minority. Cr_2NiIn has a gap after 9 states in majority and a pseudogap near 12 states in minority.

Mn2Fe(Al,Ga,In): Mn_2FeAl and Mn_2FeGa both have gaps after 9 states in majority and after 12 states in minority. Both place the Fermi energy slightly below the minority gap to generate near-half-metals as described in Table III. In Mn_2FeIn, the minority gap after 12 states becomes a pseudogap. It also has minority gaps after 9 states and after 14 states.

26 electron systems: V_2Cu(P,As,Sb), V_2Zn(Si,GeSn), Cr_2Co(P,As,Sb), Cr_2Ni(Si,Ge,Sn), Cr_2Cu(Al,Ga,In), Mn_2Fe(Si,GeSn), Mn_2Co(Al,Ga,As). Many of the 26 electron systems show gaps after 9 states, some show gaps after 12 states and a few show gaps after 14 states. None of these systems can generate the 8 μ_B moment needed to generate a half-metal using the gap after 9 states. Several, however, can generate the moment of 2 μ_B needed to generate a half-metal or near-half-metal by using a minority gap after 12 states. A moment of 2 μ_B would also be consistent with a half-metal taking advantage of a a majority gap after 14 states. In principle, a majority gap after 14 states and a minority gap after 12 combined with a moment of 2 μ_B could lead to a magnetic semiconductor. Mn_2CoAl comes close to this situation.

V_2Cu(P,As,Sb) have gaps in both spin channels after 9 states and are non-magnetic. V_2CuSb also has pseudogaps in both spin-channels after 14 states.

V_2Zn(Si,Ge,Sn) have only pseudogaps near 9 states and are also non-magnetic. None of the 26 electron systems with X=V are predicted to be half-metals or near-half-metals.

Cr_2Co(P,As,Sb) have majority gaps after 9 states and minority gaps after 12 states. Cr_2CoP also has a small minority gap after 9 states that becomes a pseudopgap for Cr_2CoAs and Cr_2CoSb. Cr_2CoP is a half-metal with a moment of 2 μ_B. Cr_2CoAs and Cr_2CoSb are near-half-metals with moments of 2.0047 and 2.0016 μ_B respectively, however they are omitted from Table III because of their positive formation energy.

Cr_2Ni(Si,Ge,Sn) are remarkable for the large gaps after 9 states in the majority channel. Cr_2NiSi and Cr_2NiGe also have smaller gaps after 9 states in the minority channel. Cr_2NiSi and Cr_2NiGe also have gaps after 12 states in minority. The Fermi energy falls just above these gaps

after 12 states giving moments of 1.89 and 1.94 μ_B respectively. Cr_2NiGe also has a minority gap after 14 states. Cr_2NiSn has a single gap after 9 states in the majority channel and a relatively small moment (0.83 μ_B). Cr_2NiSi and Cr_2NiGe satisfy our criteria for near-half-metals and are listed in Table III.

Cr_2Cu(Al,Ga,In) all show gaps after 9 states in both spin channels. In addition Cr_2CuAl has gaps after 14 states in both channels while Cr_2CuGa has gaps after 14 states in the minority channel. For all cases, however, the net moments are too small to place the Fermi energy near any of the gaps. These three systems are ferrimagnets with relatively large anti-aligned moments on the two Cr atoms.

Mn_2Fe(Si,Ge,Sn)all have minority gaps after 12 states. Mn_2FeSi and Mn_2FeSn also have pseudogaps after 9 states in majority while Mn_2FeGe has a gap after 9 states in minority. The moments (2.008 μ_B, 2.016 μ_B and 1.999 μ_B) are the right size to make all three of these systems near-half-metals (Table III); however the formation of Mn_2FeSn is positive.

Mn_2Co(Al,Ga,In) tend to have minority gaps (Al,Ga) or pseudogaps (In) after 12 states and their net moments tend to be large enough to take advantage of these gaps to make near-half-metals. Thus Mn_2CoAl is a half-metal (Table II) and Mn_2CoGa is a near-half-metal(Table III).

In addition to the gap in the minority channel after 12 states that Mn_2CoAl utilizes to make itself a half-metal, it also has a slightly negative gap in the majority channel, *i.e.* a very slight overlap between bands 14 and 15. The maximum of band 14 at the Γ point is only slightly higher than the minimum of band 15 at the X point. This situation has led some to refer this system as a "spin-gapless semiconductor"[34, 86]. In our calculation and also that of Ouardi *et al.* [28] it is a semi-metal rather than a semiconductor.

27 electron systems: The 21 systems in our database comprise: V_2Zn(P,As,Sb), Cr_2Ni(P,As,Sb), Cr_2Cu(Si,Ge,Sn), Cr_2Zn(Al,Ga,In), Mn_2Fe(P,As,Sb), Mn_2Co(Si,Ge,Sn), Mn_2Ni(Al,Ga,As). A system with 27 electrons could take advantage of a minority gap after 12 states to make a half-metal with a moment of 3 μ_B or a majority gap after 14 states to to make a half-metal with a moment of 1 μ_B.

V_2Zn(P,As,Sb): All three have gaps after 9 states in both spin channels. V_2ZnP is non-magnetic while V_2ZnAs and V_2ZnSb have relatively small moments on the V sites with ferrimagnetic alignment.Because their moments are small and there are no gaps after 12 or 14 states, these systems are very far from being half-metals.

Cr_2Ni(P,As,Sb): These three systems all generate large gaps after 9 states in the majority channel, and gaps after 12 states and after 14 states in the minority channel. The gaps after 14 states cannot be used to generate a half-metal because they are in the minority channel. The gaps after 12 states could be used to make half-metals or near-half-metals but the net moments are too small (2.03 μ_B, 1.69 μ_B and 1.29 μ_B respectively) for the Fermi energy to be near the gap.

Cr_2Cu(Si,Ge,Sn): These three systems generate gaps after 9 states in both channels and gaps (Si and Ge) or pseudogaps (Sn) after 14 states in the minority channel . There are no gaps after 12 states. The moments are too small to take advantage of the gaps after 9 states and the gaps after 14 states are in the wrong channel to be useful for making half-metals.

Cr_2Zn(Al,Ga,In): These systems only generate gaps after 14 states; Cr_2ZnAl in both channels, Cr_2ZnGa in the minority and for Cr_2ZnIn there are no gaps. The one opportunity for making a half-metal is the majority channel of Cr_2ZnAl, but the net moment is somewhat smaller (0.706 μ_B) than the 1.0 μ_B needed to make a half-metal. Pseudogaps near 9 states can be identified in both majority and minority of all three.

Mn_2Fe(P,As,Sb): These systems all generate gaps after 12 states in the minority channel and the moments have the correct value (3 μ_B)to generate half-metals (Table II). The predicted half-metal, Mn_2FeSb is omitted from Table II because it is predicted to have positive formation energy. These systems are also predicted to have pseudogaps around 9 states in both majority and minority. Mn_2FeP has a small gap after 9 states in minority.

Mn_2Co(Si,Ge,Sn): These systems all generate gaps after 12 states in the minority channel. For Mn_2CoSi and Mn_2CoGe the moment is large enough (3 μ_B)to generate a half-metal (Table II). The moment of Mn_2CoSn is too small to generate a gap. There are also gaps after 9 states in majority for Mn_2CoSi and Mn_2CoGe. This gap becomes a pseudogap for Mn_2CoSn.

Mn_2Ni(Al,Ga,As): No gaps are predicted for these three systems. Mn_2NiAl and Mn_2NiGa have pseudogaps around 14 states.

28 electron systems: The 18 systems with 28 valence electrons in our dataset comprise: Cr_2Cu(P,As,Sb), Cr_2Zn(Si,Ge,Sn), Mn_2Co(P,As,Sb), Mn_2Ni(Si,Ge,Sb), Mn_2Cu(Al,Ga,In), and Fe_2Co(Al,Ga,In). In principle, these systems could take advantage of gaps after 14 electrons to make zero moment half-metals or semiconductors, however we found no examples of such an electronic structure in a system with negative formation energy. They can also take advantage of a minority gap after 12 states to make half-metals with moments of 4 μ_B per formula unit. We found three examples of this type of electronic structure.

Two systems Cr_2Cu(P,As,Sb): These systems all have sizable gaps in majority after 9 states and smaller gaps in minority after 9 states. Cr_2CuP has a pseudogap after 14 states in minority and Cr_2CuSb has a minority pseudogap after 14 states. The moments are small.

Cr_2Zn(Si,Ge,Sn): These systems have pseudogaps near 9 states per formula unit in both spin channels. Cr_2ZnSi and Cr_2ZnGe have gaps after 14 electrons. Cr_2ZnSi has gaps in both channels so that it is predicted to be a ferrimagnetic semiconductor with zero net moment and two different gap widths. The smaller gap is a direct gap at the L point and is on the order of 0.02 eV so that XA

phase Cr_2ZnSi could be called a "spin gapless semiconductor". Cr_2ZnGe only has a gap after 14 states in one spin channel. Its net moment is almost zero (0.0004 μ_B) so that it is predicted to be a near-half-metal. Unfortunately, both of these interesting systems are predicted to have positive formation energy and hull distances in excess of 0.3 eV/atom.

Mn_2Co(P,As,Sb): Mn_2CoP and Mn_2CoAs have gaps in both channels after 9 states. All three systems have gaps after 12 states in minority. All three have the requisite moment (4 μ_B) to generate half-metals and are listed in Table II. We include details about the calculated Mn_2CoSb XA-phase in Table II even though its calculated formation energy is positive because of the controversy over the experimentally observed phase as discussed in Section III A.

Mn_2Ni(Si,Ge,Sb): These systems all have minority gaps after 12 states. Mn_2NiSi and Mn_2NiGe also have majority pseudogaps near 9 states. The moments on these systems are all too small to take advantage of the minority gap after 12 states.

Mn_2Cu(Al,Ga,In): One can identify pseudogaps near 9 states in majority in Mn_2CuAl and Mn_2CuGa along with a tiny gap after 9 states in minority in Mn_2CuGa. One can also identify pseudogaps near 14 states in both majority and minority in Mn_2CuAl.

Fe_2Co(Al,Ga,In): These systems have minority gaps after 9 states. Pseudogaps near 12 minority states can also be identified above the Fermi energy in all three systems. Even if there were a minority gap after 12 states, the moments in these systems would be too large to take advantage of it.

29 electron systems: Our database contained 18 systems with 29 valence electrons per formula unit: Cr_2Zn(P,As,Sb), Mn_2Ni(P,As,Sb), Mn_2Cu(Si,Ge,Sn), Mn_2Zn(Al,Ga,In), Fe_2Co(Si,Ge,Sn), and Fe_2Ni(Al,Ga,In). In principle, a system with 29 electrons per formula unit could utilize a minority gap after 9, 12, or 14 states together with moments of 9 μ_B, 5 μ_B, or 1 μ_B respectively, to make a half-metal. In practice we only find one 29 electron half-metal, Mn_2CuSi, with a moment of 1 μ_B.

Cr_2Zn(P,As,Sb): These systems all showed gaps after 9 states and 15 states in the minority channel. Cr_2ZnP also has a gap after 9 states in the majority channel and a pseudogap after 14 states in minority. Cr_2ZnAs also has a pseudogap near 9 states and a gap after 14 states in majority. In principle the gap after 14 states in the majority could be utilized to make a half-metal, but the moment is too small (0.47 μ_B). Cr_2ZnSb has in addition to the minority gaps after 9 and 15 states, a pseudogap near 9 states in majority. The gap after 15 states observed in the minority channel of Cr_2Zn(P,As,Sb) is unusual and can be traced to a singly degenerate state at Γ that is usually band 15 or band 17 dropping below a triply degenerate state.

Mn_2Ni(P,As,Sb): These three systems have gaps (Mn_2NiP) or pseudogaps (Mn_2Ni(As,Sb)) near 12 states in the minority channel, but the moments are all much less than the 5 μ_B that would be necessary to make a half-metal. In addition, pseudogaps near 9 states in majority and 14 states in minority can be identified for Mn_2NiP.

Mn_2Cu(Si,Ge,Sn): all have gaps after 9 states in both the majority and minority channels. Mn_2CuSi also has a minority pseudogap near 12 states and a minority gap after 14 states. The system uses the minority gap after 14 states to make a half-metal (Table II).

Mn_2Zn(Al,Ga,In): all have small moments and no gaps. Pseudogaps in both channels near 9 states can be identified.

Fe_2Co(Si,Ge,Sn): all have moments near 5 μ_B. However instead of gaps after 12 states in minority there are pseudogaps. All three have gaps after 9 states in minority. Fe_2CoSi also has a pseudogap near 9 states in majority.

Fe_2Ni(Al,Ga,In): also all have moments near 5 μ_B, but the only gaps are after 9 states in the minority channel. Fe_2NiAl has a minority pseudogap near 12 states and majority pseudogaps near 14 and 16 states. Fe_2NiGa has majority pseudogaps near 9 states and 16 states.

30 electron systems: The 15 systems in our database with 30 electrons are: Mn_2Cu(P,As,Sb), Mn_2Zn(Si,Ge,Sn), Fe_2Co(P,As,Sb), Fe_2Ni(Si,Ge,Sn), and Fe_2Cu(Al,Ga,In). In principle gaps after 14, 12, or 9 states could be used to make half-metals with moments of 2 μ_B , 6 μ_B or 12 μ_B respectively. In practice we find one negative-formation-energy near-half-metal with a moment near 2 μ_B.

Mn_2Cu(P,As,Sb): These all have gaps after 9 states in both majority and minority. Mn_2CuP also has a gap after 14 states in the minority channel. The moment is nearly 2 μ_B which makes it a near-half-metal.

Mn_2Zn(Si,Ge,Sn): These systems have pseudogaps in both spin channels near 9 states. Mn_2ZnSi also has a gap after 14 electrons in the minority channel and a spin moment of exactly 2 μ_B which makes it a half-metal. Unfortunately, its calculated formation energy is positive. Mn_2ZnGe and Mn_2ZnSn do not have gaps in the DOS at the experimental lattice constant. If, however, their lattices are significantly contracted, the gap after 14 states reappears and the Fermi energy falls into the gap.

Fe_2Co(P,As,Sb): These all have gaps after 9 electrons in the minority channel and pseudogaps near 12 states also in the minority channel. The moments are large enough (5.76 μ_B, 5.95 μ_B, 5.93 μ_B respectively) to place the Fermi energy in the vicinity of the 12 state pseudogap, but because there is not really a gap, these are not near-half-metals.

Fe_2Ni(Si,Ge,Sn): These all have gaps after 9 states in the minority. Fe_2NiSi and Fe_2NiGe also have majority gaps after 9 states. Fe_2NiSi also has a minority gap after 12 states while Fe_2NiGe has a minority pseudogap after 12 states. The moments are relatively large (4.78 μ_B, 5.09 μ_B, 5.23 μ_B respectively) but not large enough (6 μ_B would have been required) to make them half-metals

or near-half-metals.

Fe_2Cu(Al,Ga,In): These all have relatively large minority gaps after 9 states and small majority gaps after 14 states (Fe_2CuAl and Fe_2CuGa) or after 16 states (Fe_2CuIn). Fe_2CuIn also has a pseudogap after 14 states in the majority. The majority gaps after 14 states cannot be used to make a half-metal and although the majority gap after 16 could be used, the moment is too large, $4.84\mu_B$ rather than $2\mu_B$.

31 electron systems: The 15 systems in our database with 31 electrons comprise Mn_2Zn(P,As,Sb), Fe_2Ni(P,As,Sb), Fe_2Cu(Si,Ge,Sn), Fe_2Zn(Al,Ga,In) and Co_2Ni(Al,Ga,In). Compounds with 31 electrons could, in principle, take advantage of a minority gap after 14, 12 or 9 states with a moment of $3\mu_B$, $7\mu_B$, or $13\mu_B$ respectively. In addition, we find one example of a gap after 15 states which would allow a half-metal with a moment of 1 μ_B. In practice, we find no 31-electron half-metals or near-half-metals with negative formation energy.

Mn_2Zn(P,As,Sb): All three systems have gaps after 9 states in minority. Mn_2ZnP also has a gap after 9 states in majority while Mn_2ZnAs has a pseudogap near 9 states in majority. Mn_2ZnP has a pseudogap near 14 states in minority. Mn_2ZnAs has a tiny minority gap after 15 states and a moment (1.001 μ_B) that places the Fermi energy very near this gap. Unfortunately, its formation energy is positive. Mn_2ZnSb has a similar electronic structure and moment, but the tiny gap in Mn_2ZnAs is replaced by a pseudogap in Mn_2ZnSb.

Fe_2Ni(P,As,Sb): These all have minority gaps after 9 states. Fe_2NiP also has a minority gap after 12 states while Fe_2NiAs and Fe_2NiSb have pseudogaps after 12 states. The moments are too small to take advantage of the gap or pseudogaps after 12 states.

Fe_2Cu(Si,Ge,Sn): These all have gaps after 9 states in both spin channels, with the minority gap being larger than the majority gap. In addition, Fe_2CuSi and Fe_2CuSn have narrow gaps after 14 states in the majority. None of these gaps are near the Fermi energy.

Fe_2Zn(Al,Ga,In): These systems have gaps (Al) or pseudogaps (Ga,In) at 14 states in minority. The moments are to large to place the Fermi energy near these gaps or pseudogaps.

Co_2Ni(Al,Ga,In): These systems have numerous gaps and pseudogaps. All three have narrow, deep, pseudogaps near 14 states in minority and have moments (2.99, 3.02, 3.13)μ_B that place the Fermi energy in the pseudogaps. They are not "near-half-metals" according to our definition. In addition, all three have minority pseudogaps near 12 states. They all also have gaps after 9 states in minority. Co_2NiAl has a gap after 14 states in majority. Co_2NiGa has a gap after 9 states in majority and pseudogaps near 14 and 16 states in majority.

32 electron systems: The 12 systems with 32 electrons in our database include Fe_2Cu(P,As,Sb), Fe_2Zn(Si,Ge,Sn), Co_2Ni(Si,Ge,Sn), and Co_2Cu(Al,Ga,In).

Fe_2Cu(P,As,Sb): These systems all have gaps after 9 states in both spin channels and pseudogaps after 14 states in the minority channel. Their moments are all greater than 4 μ_B, and the moment of Fe_2CuP is 4.018 μ_B, quite close the the value of 4 needed to generate a half-metal. Unfortunately, the Fermi energy is on the edge of a pseudogap rather than a gap.

Fe_2Zn(Si,Ge,Sn): The 31 electron Fe_2ZnZ XA compounds have pseudogaps rather than gaps near 9 states in both spin channels, but similar to the 31-electron Fe_2CuZ systems, they have pseudogaps near 14 states in the minority channel. The pseudogap near 14 states in Fe_2ZnSi is remarkable in that the DOS plots appear to show a gap after 14 states. Its moment (3.982 μ_B) is close enough to 4 that we would classify Fe_2ZnSi as a near-half-metal and include it in Table III because it also has a negative formation energy. However, bands 14 and 15 cross between X and W, spoiling the gap.

Co_2Ni(Si,Ge,Sn): These all have gaps after nine states in both spin channels and pseudogaps near 12 states in minority. Their moments are too small (2.51 μ_B, 2.56 μ_B, 2.70 μ_B) to place the Fermi energy near the pseudogaps. None are half-metals or near-half-metals.

Co_2Cu(Al,Ga,In) These all have gaps after 9 states in the minority channel. None are half-metals or near-half-metals.

33 electron systems: The 12 systems with 33 electrons in our database include Fe_2Zn(P,As,Sb), Co_2Ni(P,As,Sb), Co_2Cu(Si,Ge,Sn), and Co_2Zn(Al,Ga,In). These systems would need a moment of 5 μ_B to utilize a gap after 14 states to make a half-metal. They have neither the gaps nor the moment.

Fe_2Zn(P,As,Sb): These systems have either gaps (P,As) or pseudogaps after 9 states in both spin channels.

Co_2Ni(P,As,Sb): These systems all have gaps after 9 states in both spin channels. Pseudogaps near 12 states in minority can also be identified for all three systems.

Co_2Cu(Si,Ge,Sn): These systems also have gaps after 9 states in both channels. Two (Si,Ge) have pseudogaps after 12 states in both spin channels.

Co_2Zn(Al,Ga,In): No gaps or convincing pseudogaps were observed in these systems.

34 electron systems: The 9 systems in our database with 34 electrons include Co_2Cu(P,As,Sb), Co_2Zn(Si,Ge,Sn) and Ni_2Cu(Al,Ga,In).

Co_2Cu(P,As,Sb): These systems have gaps after 9 states in both channels. Co_2CuP also has a majority gap after 12 states which becomes a pseudogap for the other two compounds. The moments are not nearly large enough to place the Fermi energy near the gaps or pseudogaps.

Co_2Zn(Si,Ge,Sn): These systems all have pseudogaps near 9 states in both spin channels and also a pseudogap near 12 states in the minority channel.

Ni_2Cu(Al,Ga,In): These systems are non-magnetic and have no gaps. Ni_2CuAl and Ni_2CuGa have pseudogaps near 12 states in both channels. Ni_2CuGa and Ni_2CuIn have pseudogaps after 9 states in both channels.

35 electron systems: The 9 systems in our database with 35 electrons include Co_2Zn(P,As,Sb), Ni_2Cu(Si,Ge,Sn) and Ni_2Zn(Al,Ga,In). A system with 35 electrons would need a moment of 7 μ_B to take advantage of a gap after 14 states in minority. Such moments would be unlikely in these systems because the d-bands are nearly filled for Co and especially for Ni.

Co_2Zn(P,As,Sb): These systems are magnetic with moments relatively small moments, (2.4 μ_B, 2.5 μ_B, and 2.7 μ_B). Co_2ZnP and Co_2ZnAs have gaps after 9 states in both spin channels while Co_2ZnSb has pseudogaps near 9 states in both spin channels. Pseudogaps near 14 states can be identified in all three systems.

Ni_2Cu(Si,Ge,Sn): These are all non-magnetic and have gaps after 9 states in each of the identical spin channels. Pseudogaps near 12 states can be identified in all three as well as near 14 states in Ni_2CuSn.

36 electron systems: The 6 systems in our database with 36 electrons include Ni_2Cu(P,As,Sb) and Ni_2Zn(Si,Ge,Sn). None of these systems are magnetic.

Ni_2Cu(P,As,Sb): These have gaps after 9 states and pseudogaps near 12 states and 14 states.

Ni_2Zn(Si,Ge,Sn): These have pseudogaps near 14 states.

37 electron systems: The 6 systems in our database with 37 electrons are Ni_2Zn(P,As,Sb) and Cu_2Zn(Al,Ga,In). None of these 6 systems has a magnetic moment and therefore cannot be half-metals.

Ni_2Zn(P,As,Sb): Ni_2ZnP and Ni_2ZnAs have gaps after 9 states. Ni_2ZnSb has a pseudogap near 9 states. Pseudogaps after 14 states can be identified for all three.

Cu_2Zn(Al,Ga,In): These systems have no gaps.

38 electron systems: The three systems in our database with 38 electrons are Cu_2Zn(Si,Ge,Sn). They have neither moments nor gaps.

39 electron systems: The three systems in our database with 39 electrons are Cu_2Zn(P,As,Sb). They have neither moments nor gaps.

V. CONCLUSION

We have performed extensive first-principles calculations on 405 inverse-Heusler compounds X_2YZ, where X=Sc, Ti, V, Cr, Mn, Fe, Co, Ni, or Cu; Y=Ti, V, Cr, Mn, Fe, Co, Ni, Cu, or Zn; and Z=Al, Ga, In, Si, Ge, Sn, P, As, or Sb with a goal of identifying materials of interest for spintronic applications. We identified 14 semiconductors with negative formation energy. These are listed in Table I. We identified many half-metals and near-half-metals. Those half-metals and near-half-metals that we identified and that have negative formation energy are listed in Tables II and III. respectively.

We have identified four half-metals and six near-half-metals that meet a criterion for stability that we estimated based on a study of the hull distances of known XA phases. Seven of these ten predicted phases have not (to our knowledge) been observed experimentally.

In establishing our stability criterion, we analyzed the experimental and theoretical data for several reported XA phases (Mn_2CoIn, Mn_2CoSb, Mn_2CoSn, Mn_2RuSn) and tentatively concluded that they are not XA but are more likely a disordered phase such as $L2_1B$. We recommend more extensive studies of these materials.

The ten half-metallic or near-half-metallic phases that we identified as reasonably likely to be stable, are all Slater-Pauling phases, *i.e.* they have a gap in the density of states after three states per atom in one of the two spin channels, and the Fermi energy is in or near this gap. Many half-metallic and near-half-metallic phases based on a gap after 9 states per formula unit (2.25 states per atom) were identified, but we estimate that other phases or combination of phases are likely to be more stable in equilibrium.

ACKNOWLEDGMENTS

The authors acknowledge support from the National Science Foundation through grants DMREF-1235230 and DMREF-1235396. JH and CW (OQMD stability and SQS calculations) acknowledge support via ONR STTR N00014-13-P-1056. The authors also acknowledge Advanced Research Computing Services at the University of Virginia and High Performance Computing staff from the Center for Materials for Information Technology at the University of Alabama for providing technical support that has contributed to the results in this paper. The computational work was done using the High Performance Computing Cluster at the Center for Materials for Information Technology, University of Alabama, resources of the National Energy Research Scientific Computing Center (NERSC), a DOE Office of Science User Facility supported by the Office of Science of the U.S. Department of Energy under Contract No. DE-AC02-05CH11231 and the Rivanna high-performance cluster at the University of Virginia.

[1] I. Žutić, J. Fabian, and S. Das Sarma, Rev. Mod. Phys. **76**, 323 (2004).
[2] A. Hirohata and K. Takanashi, Journal of Physics D: Applied Physics **47**, 193001 (2014).
[3] Y. Ando, Japanese Journal of Applied Physics **54**, 070101 (2015).
[4] C. Felser, G. Fecher, and B. Balke, Angewandte Chemie International Edition **46**, 668 (2007).
[5] M. I. Katsnelson, V. Y. Irkhin, L. Chioncel, A. I. Lichtenstein, and R. A. de Groot, Rev. Mod. Phys. **80**, 315 (2008).
[6] R. A. de Groot, F. M. Mueller, P. G. v. Engen, and

K. H. J. Buschow, Phys. Rev. Lett. **50**, 2024 (1983).
[7] I. Galanakis, P. H. Dederichs, and N. Papanikolaou, Phys. Rev. B **66**, 134428 (2002).
[8] I. Galanakis, P. H. Dederichs, and N. Papanikolaou, Phys. Rev. B **66**, 174429 (2002).
[9] H. C. Kandpal, C. Felser, and R. Seshadri, Journal of Physics D: Applied Physics **39**, 776 (2006).
[10] I. Galanakis, P. Mavropoulos, and P. H. Dederichs, Journal of Physics D: Applied Physics **39**, 765 (2006).
[11] I. Galanakis, Journal of Physics: Condensed Matter **16**, 3089 (2004).
[12] S. Skaftouros, K. Özdoğan, E. Şaşıoğlu, and I. Galanakis, Phys. Rev. B **87**, 024420 (2013).
[13] J. Kübler, Journal of Physics: Condensed Matter **18**, 9795 (2006).
[14] J. Kübler, G. H. Fecher, and C. Felser, Phys. Rev. B **76**, 024414 (2007).
[15] C. G. F. Blum, C. A. Jenkins, J. Barth, C. Felser, S. Wurmehl, G. Friemel, C. Hess, G. Behr, B. Bchner, A. Reller, S. Riegg, S. G. Ebbinghaus, T. Ellis, P. J. Jacobs, J. T. Kohlhepp, and H. J. M. Swagten, Applied Physics Letters **95**, 161903 (2009).
[16] C. Felser, L. Wollmann, S. Chadov, G. H. Fecher, and S. S. P. Parkin, APL Materials **3**, 041518 (2015).
[17] S. Tsunegi, Y. Sakuraba, M. Oogane, H. Naganuma, K. Takanashi, and Y. Ando, Applied Physics Letters **94**, 252503 (2009).
[18] N. Tezuka, N. Ikeda, F. Mitsuhashi, and S. Sugimoto, Applied Physics Letters **94**, 162504 (2009).
[19] H.-X. Liu, Y. Honda, T. Taira, K.-i. Matsuda, M. Arita, T. Uemura, and M. Yamamoto, Applied Physics Letters **101**, 132418 (2012).
[20] H.-X. Liu, T. Kawami, K. Moges, T. Uemura, M. Yamamoto, F. Shi, and P. M. Voyles, Journal of Physics D: Applied Physics **48**, 164001 (2015).
[21] D. C. Worledge and T. H. Geballe, Journal of Applied Physics **88**, 5277 (2000).
[22] P. LeClair, J. K. Ha, H. J. M. Swagten, J. T. Kohlhepp, C. H. van de Vin, and W. J. M. de Jonge, Applied Physics Letters **80**, 625 (2002).
[23] T. Iwase, Y. Sakuraba, S. Bosu, K. Saito, S. Mitani, and K. Takanashi, Applied Physics Express **2**, 063003 (2009).
[24] T. M. Nakatani, T. Furubayashi, S. Kasai, H. Sukegawa, Y. K. Takahashi, S. Mitani, and K. Hono, Applied Physics Letters **96**, 212501 (2010).
[25] Y. K. Takahashi, A. Srinivasan, B. Varaprasad, A. Rajanikanth, N. Hase, T. M. Nakatani, S. Kasai, T. Furubayashi, and K. Hono, Applied Physics Letters **98**, 152501 (2011).
[26] J. Sato, M. Oogane, H. Naganuma, and Y. Ando, Applied Physics Express **4**, 113005 (2011).
[27] S. Chadov, T. Graf, K. Chadova, X. Dai, F. Casper, G. H. Fecher, and C. Felser, Phys. Rev. Lett. **107**, 047202 (2011).
[28] S. Ouardi, G. H. Fecher, C. Felser, and J. Kübler, Phys. Rev. Lett. **110**, 100401 (2013).
[29] W. H. Butler, A. W. Ghosh, *et al.*, "Heuslers home," http://heusleralloys.mint.ua.edu/ (2016).
[30] J. Ma, V. I. Hegde, K. Munira, Y. Xie, S. Keshavarz, D. T. Mildebrath, C. Wolverton, A. W. Ghosh, and W. H. Butler, Phys. Rev. B **95**, 024411 (2017).
[31] J. C. Slater and G. F. Koster, Phys. Rev. **94**, 1498 (1954).
[32] J. C. Slater, Journal of Applied Physics **8**, 385 (1937).
[33] L. Pauling, Phys. Rev. **54**, 899 (1938).
[34] S. Skaftouros, K. Özdoğan, E. Şaşıoğlu, and I. Galanakis, Applied Physics Letters **102**, 022402 (2013).
[35] I. Galanakis, K. Özdoğan, E. Şaşıoğlu, and S. Blügel, Journal of Applied Physics **115**, 093908 (2014).
[36] N. Lakshmi, A. Pandey, and K. Venugopalan, Bulletin of Materials Science **25**, 309 (2002).
[37] M. Meinert, J.-M. Schmalhorst, C. Klewe, G. Reiss, E. Arenholz, T. Böhnert, and K. Nielsch, Phys. Rev. B **84**, 132405 (2011).
[38] J. Winterlik, G. H. Fecher, B. Balke, T. Graf, V. Alijani, V. Ksenofontov, C. A. Jenkins, O. Meshcheriakova, C. Felser, G. Liu, S. Ueda, K. Kobayashi, T. Nakamura, and M. Wójcik, Phys. Rev. B **83**, 174448 (2011).
[39] Y. Xin, H. Hao, Y. Ma, H. Luo, F. Meng, H. Liu, E. Liu, and G. Wu, Intermetallics **80**, 10 (2017).
[40] G. D. Liu, X. F. Dai, H. Y. Liu, J. L. Chen, Y. X. Li, G. Xiao, and G. H. Wu, Phys. Rev. B **77**, 014424 (2008).
[41] F. Ahmadian and A. Salary, Intermetallics **46**, 243 (2014).
[42] A. Jakobsson, P. Mavropoulos, E. Şaşıoğlu, S. Blügel, M. Ležaić, B. Sanyal, and I. Galanakis, Phys. Rev. B **91**, 174439 (2015).
[43] J. Saal, S. Kirklin, M. Aykol, B. Meredig, and C. Wolverton, JOM **65**, 1501 (2013).
[44] S. Kirklin, J. E. Saal, B. Meredig, A. Thompson, J. W. Doak, M. Aykol, S. Rühl, and C. Wolverton, npj Computational Materials **1**, 15010 (2015).
[45] G. Kresse and J. Furthmller, Computational Materials Science **6**, 15 (1996).
[46] P. E. Blöchl, Phys. Rev. B **50**, 17953 (1994).
[47] J. P. Perdew, K. Burke, and M. Ernzerhof, Phys. Rev. Lett. **77**, 3865 (1996).
[48] H. J. Monkhorst and J. D. Pack, Phys. Rev. B **13**, 5188 (1976).
[49] P. E. Blöchl, O. Jepsen, and O. K. Andersen, Phys. Rev. B **49**, 16223 (1994).
[50] K. zdogan and I. Galanakis, Journal of Magnetism and Magnetic Materials **321**, L34 (2009).
[51] H. Luo, Z. Zhu, L. Ma, S. Xu, X. Zhu, C. Jiang, H. Xu, and G. Wu, Journal of Physics D: Applied Physics **41**, 055010 (2008).
[52] M. Meinert, J.-M. Schmalhorst, and G. Reiss, Journal of Physics: Condensed Matter **23**, 116005 (2011).
[53] B. Xu, M. Zhang, and H. Yan, physica status solidi b **248**, 2870 (2011).
[54] M. Pugaczowa-Michalska, Intermetallics **24**, 128 (2012).
[55] N. Kervan and S. Kervan, Journal of Physics and Chemistry of Solids **72**, 1358 (2011).
[56] P. Klaer, C. A. Jenkins, V. Alijani, J. Winterlik, B. Balke, C. Felser, and H. J. Elmers, Applied Physics Letters **98** (2011), 10.1063/1.3592802.
[57] V. Alijani, J. Winterlik, G. H. Fecher, and C. Felser, Applied Physics Letters **99** (2011), 10.1063/1.3665260.
[58] O. Meshcheriakova, S. Chadov, A. K. Nayak, U. K. Rößler, J. Kübler, G. André, A. A. Tsirlin, J. Kiss, S. Hausdorf, A. Kalache, W. Schnelle, M. Nicklas, and C. Felser, Phys. Rev. Lett. **113**, 087203 (2014).
[59] A. Zunger, S.-H. Wei, L. G. Ferreira, and J. E. Bernard, Phys. Rev. Lett. **65**, 353 (1990).
[60] A. Van de Walle, P. Tiwary, M. De Jong, D. Olmsted, M. Asta, A. Dick, D. Shin, Y. Wang, L.-Q. Chen, and Z.-K. Liu, Calphad **42**, 13 (2013).

[61] A. van de Walle, Calphad **33**, 266 (2009).
[62] A. R. Akbarzadeh, V. Ozolins, and C. Wolverton, Advanced Materials **19**, 3233 (2007).
[63] S. Kirklin, B. Meredig, and C. Wolverton, Advanced Energy Materials **3**, 252 (2013).
[64] G. Bergerhoff and I. D. Brown, International Union of Crystallography, Chester **360**, 77 (1987).
[65] A. Belsky, M. Hellenbrandt, V. L. Karen, and P. Luksch, Acta Crystallographica Section B **58**, 364 (2002).
[66] M. Yin, P. Nash, and S. Chen, Intermetallics **57**, 34 (2015).
[67] G. Kreiner, A. Kalache, S. Hausdorf, V. Alijani, J.-F. Qian, G. Shan, U. Burkhardt, S. Ouardi, and C. Felser, Zeitschrift fr anorganische und allgemeine Chemie **640**, 738 (2014).
[68] H. Luo, G. Liu, Z. Feng, Y. Li, L. Ma, G. Wu, X. Zhu, C. Jiang, and H. Xu, Journal of Magnetism and Magnetic Materials **321**, 4063 (2009).
[69] S. Bakkar and D. Mazumdar, (2017), unpublished.
[70] X. Dai, G. Liu, L. Chen, J. Chen, and G. Wu, Solid State Communications **140**, 533 (2006).
[71] K. Endo, T. Kanomata, H. Nishihara, and K. Ziebeck, Journal of Alloys and Compounds **510**, 1 (2012).
[72] L. Yang, B. Liu, H. Luo, F. Meng, H. Liu, E. Liu, W. Wang, and G. Wu, Journal of Magnetism and Magnetic Materials **382**, 247 (2015).
[73] W. H. Butler, C. K. Mewes, C. Liu, and T. Xu, arXiv preprint arXiv:1103.3855 (2011).
[74] T. Nakamichi and H. Itoh, Journal of the Physical Society of Japan **38**, 1781 (1975).
[75] K. Buschow and P. van Engen, Journal of Magnetism and Magnetic Materials **25**, 90 (1981).
[76] K. Buschow, P. van Engen, and R. Jongebreur, Journal of Magnetism and Magnetic Materials **38**, 1 (1983).
[77] R. Y. Umetsu, K. Kobayashi, A. Fujita, R. Kainuma, and K. Ishida, Journal of Applied Physics **103** (2008), 10.1063/1.2836677.
[78] S. Fujii, S. Ishida, and S. Asano, Journal of the Physical Society of Japan **63**, 1881 (1994).
[79] K. Miyamoto, A. Kimura, Y. Miura, M. Shirai, M. Ye, Y. Cui, K. Shimada, H. Namatame, M. Taniguchi, Y. Takeda, Y. Saitoh, E. Ikenaga, S. Ueda, K. Kobayashi, and T. Kanomata, Phys. Rev. B **79**, 100405 (2009).
[80] M. A. I. Nahid, M. Oogane, H. Naganuma, and Y. Ando, Japanese Journal of Applied Physics **48**, 083002 (2009).
[81] R. Sobczak, Monatshefte für Chemie / Chemical Monthly **107**, 977 (1976).
[82] M. R. Paudel, C. S. Wolfe, H. Patton, I. Dubenko, N. Ali, J. A. Christodoulides, and S. Stadler, Journal of Applied Physics **105**, 013716 (2009), 10.1063/1.3054291.
[83] E. Shreder, S. V. Streltsov, A. Svyazhin, A. Makhnev, V. V. Marchenkov, A. Lukoyanov, and H. W. Weber, Journal of Physics: Condensed Matter **20**, 045212 (2008).
[84] A. Carbonari, R. Saxena, W. P. Jr., J. M. Filho, R. Attili, M. Olzon-Dionysio, and S. de Souza, Journal of Magnetism and Magnetic Materials **163**, 313 (1996).
[85] B. Varaprasad, A. Rajanikanth, Y. Takahashi, and K. Hono, Acta Materialia **57**, 2702 (2009).
[86] X. L. Wang, Phys. Rev. Lett. **100**, 156404 (2008).